ϕ^4 lattice model with cubic symmetry in three dimensions: Renormalization group flow and first-order phase transitions

Martin Hasenbusch ⬤

Institut für Theoretische Physik, Universität Heidelberg, Philosophenweg 19, 69120 Heidelberg, Germany

We study the three-component ϕ^4 model on the simple cubic lattice in the presence of a cubic perturbation. To this end, we perform Monte Carlo simulations in conjunction with a finite-size scaling analysis of the data. The analysis of the renormalization group (RG) flow of a dimensionless quantity provides us with the accurate estimate $Y_4 - \omega_2 = 0.000\,81(7)$ for the difference of the RG eigenvalue Y_4 at the O(3)-symmetric fixed point and the correction exponent ω_2 at the cubic fixed point. We determine an effective exponent ν_{eff} of the correlation length that depends on the strength of the breaking of the O(3) symmetry. Field theory predicts that depending on the sign of the cubic perturbation, the RG flow is attracted by the cubic fixed point, or runs to an ever increasing amplitude, indicating a fluctuation-induced first-order phase transition. We demonstrate directly the first-order nature of the phase transition for a sufficiently strong breaking of the O(3) symmetry. We obtain accurate results for the latent heat, the correlation length in the disordered phase at the transition temperature, and the interface tension for interfaces between one of the ordered phases and the disordered phase. We study how these quantities scale with the RG flow, allowing quantitative predictions for weaker breaking of the O(3) symmetry.

I. INTRODUCTION

We study the ϕ^4 model with a cubic anisotropy in three dimensions. We focus on the case of $N = 3$ components of the field, which is particularly interesting, since it is the experimentally most relevant case and the cubic perturbation is very close to marginal at the O(3)-symmetric fixed point. The model has been studied intensively over the last five decades, using field-theoretic methods such as the ϵ expansion and perturbation theory in three dimensions fixed. For a review see, for example, Sec. 11.3 of Ref. [1]. Note that in structural transitions, in addition to $N = 3$, $N = 4$ might be experimentally realized [2]. Recently the ϵ expansion has been extended to six loop [3]. Based on this, a huge set of operator dimensions have been computed in Ref. [4].

In the field-theoretic setting, the reduced continuum Hamiltonian with two quartic couplings

$$\mathcal{H} = \int d^d x \left\{ \frac{1}{2} \sum_{i=1}^N \left[(\partial_\mu \phi_i)^2 + r \phi_i^2 \right] + \frac{1}{4!} \sum_{i,j=1}^N (u + v \delta_{ij}) \phi_i^2 \phi_j^2 \right\}, \tag{1}$$

where ϕ_i is a real number, is studied [see, for example, Eq. (11.10) of Ref. [1]]. Flow equations in a two-dimensional parameter space (u, v) are discussed. For $v = 0$, the theory is O(N) symmetric, while for finite v, the theory has only cubic symmetry. The qualitative features of the flow are well understood. There are four fixed points: the Gaussian $(u, v) = (0, 0)$, the decoupled Ising $(0, v^*)$, the O(N) symmetric $(u, v) = (u^*, 0)$, and the fixed point with cubic symmetry only $(u, v) = (u_c, v_c)$, where $v_c > 0$. The Gaussian and the decoupled Ising (DI) fixed points are unstable for all values of N and $N > 1$, respectively. The O(N)-symmetric

fixed point is unstable for $N \geqslant N_c$ in one direction, breaking the O(N) symmetry. Recent field-theoretic estimates give robustly N_c slightly smaller than 3. The result $N_c < 3$ is supported by the fact that in a finite-size scaling analysis of Monte Carlo data for the improved ϕ^4 model on the simple cubic lattice the authors find $Y_4 = 0.013(4)$ for $N = 3$ [5]. In Ref. [6], $Y_4 = 0.0142(6)$ had been obtained. The rigorous bound $Y_4 > 3 - 2.990\,56$ for $N = 3$ was recently established by using the conformal bootstrap (CB) method [7]. Note that Y_4 is the renormalization group (RG) exponent of the cubic perturbation at the O(N)-symmetric fixed point and $Y_4 > 0$ means that the perturbation is relevant and hence the RG fixed point is unstable. The cubic fixed point is stable for $N \geqslant N_C$ and for $v > 0$ the flow runs into the cubic fixed point. On the contrary, for $v < 0$, the flow runs to ever larger violations of the O(N) symmetry and no fixed point is reached. Instead, a fluctuation-induced first-order phase transition is expected.

In Ref. [8] the authors pointed out that the slow RG flow, related with the small value of Y_4, requires the knowledge of the RG flow also at finite distances from the fixed points in order to interpret experimental results. Slow in this context means that the couplings change only by little, when the length scale is varied over a range that can be studied in experiments or in simulations. Just to get an idea: Take a sample of a material of linear size 10^{-1} m and a lattice constant of 10^{-10} m. Then the amplitude of a cubic perturbation in the neighborhood of the O(3)-symmetric fixed point only increases by a factor of $(10^9)^{0.0142} = 1.34\ldots$ going from the microscopic to the macroscopic scale, where we have taken the estimate of Y_4 for $N = 3$ obtained in Ref. [6]. In Ref. [8] it is demonstrated that the RG flow rapidly collapses on a line connecting the decoupled Ising, the cubic, and the O(3)-symmetric fixed points. Also for $v < 0$, the RG flow

remains slow on the continuation of this line for a relatively large range of v. It follows that the first-order transition is very weak for a large range of the parameters, such that in experiments it appears as a continuous transition, albeit with critical exponents slightly different from those of the O(3)-symmetric fixed point. This picture has been worked out in Ref. [8] by using the coefficients of the six-loop ϵ expansion obtained in Ref. [3]. For related work on systems with competing order parameters by the same authors, see [9–11]. Here we corroborate and extend these results by using Monte Carlo simulations and finite-size scaling (FSS) methods.

We build on Ref. [6], where we performed large-scale Monte Carlo simulations of a lattice version of the ϕ^4 model. We studied the cases $N = 3$ and 4, focusing on the neighborhood of the O(N)-symmetric and the cubic fixed points. By using finite-size scaling, we computed accurate estimates of critical exponents for the cubic fixed point. In the case $N = 3$ these differ only by little from their O(N)-symmetric counterparts.

In this work, we extend the study of the RG flow towards stronger violations of the O(3) symmetry. On the one hand, we make contact with the decoupled Ising fixed point. On the other hand, for $v < 0$, for large violations of the O(3) symmetry, we demonstrate directly the first-order nature of the transition. In our simulations we determine characteristic quantities such as the latent heat, the correlation length at the transition temperature, and the interface tension between the disordered and one of the ordered phases. We study how these quantities scale with the RG flow. This way, quantitative predictions can be made for all $v < 0$.

The outline of the paper is the following: In the next section we define the model and the observables that we measure. In Sec. III we discuss the basic ideas and objectives of our study. The numerical results for the RG flow are analyzed in Sec. IV. We determine effective critical exponents of the correlation length for different strengths of the symmetry breaking in Sec. V. In Sec. VI we discuss our numerical results for the first-order transition. In Sec. VII we summarize and conclude. In Appendix A we summarize technical aspects of our numerical analysis and explain how we arrive at final results. In Appendix B we summarize basic analytic results derived from the β function.

II. THE MODEL AND OBSERVABLES

Here we study the same reduced Hamiltonian and observables as in Ref. [6]. For completeness let us recall the definitions. We study a discretized version of the continuum Hamiltonian (1), which is considered in field theory. We extend the reduced Hamiltonian of the ϕ^4 model on a simple cubic lattice [see, for example, Eq. (1) of Ref. [12]] by a term proportional to the traceless symmetric combination of four instances of the field [see, for example, Eq. (7) of Ref. [5]]

$$\sum_a Q_{4,aaaa}(\vec{\phi}_x) = \sum_a \phi_{x,a}^4 - \frac{3}{N+2}(\vec{\phi}_x^2)^2, \qquad (2)$$

with cubic symmetry, breaking O(N) invariance. Actually, this choice goes back to Ref. [13], where perturbations at the O(N)-symmetric fixed point were studied to leading order in

the ϵ expansion. We get

$$\mathcal{H}(\{\vec{\phi}\}) = -\beta \sum_{\langle xy \rangle} \vec{\phi}_x \cdot \vec{\phi}_y + \sum_x \left[\vec{\phi}_x^2 + \lambda (\vec{\phi}_x^2 - 1)^2 \right.$$
$$\left. + \mu \left(\sum_a \phi_{x,a}^4 - \frac{3}{N+2}(\vec{\phi}_x^2)^2 \right) \right], \qquad (3)$$

where $\vec{\phi}_x$ is a vector with N real components. The subscript a denotes the components of the field and $\{\vec{\phi}\}$ is the collection of the fields at all sites x. We label the sites of the simple cubic lattice by $x = (x_0, x_1, x_2)$, where $x_i \in \{0, 1, \ldots, L_i - 1\}$. Furthermore, $\langle xy \rangle$ denotes a pair of nearest neighbors on the lattice. In our study, the linear lattice size $L = L_0 = L_1 = L_2$ is equal in all three directions throughout. We employ periodic boundary conditions. The real numbers β, λ, and μ are the parameters of the model. Note that here λ and μ take over the role of the parameters u and v of the continuum Hamiltonian (1). In the Hamiltonian (3) we take Eq. (2) instead of simply $\sum_a \phi_{x,a}^4$, analogous to Eq. (1), to achieve

$$\left\langle A_{O(N)}(\{\vec{\phi}\}) \sum_{a,x} Q_{4,aaaa}(\vec{\phi}_x) \right\rangle_{\mu=0} = 0, \qquad (4)$$

where the estimator $A_{O(N)}$ is O(N) invariant, while for an estimator with cubic symmetry, breaking O(N) invariance, we get in general a finite value.

A. Decoupled systems

In Eq. (3) the components of the field decouple for $\lambda - \frac{3}{N+2}\mu = 0$. Since the term $\sum_x \vec{\phi}_x^2$ has the factor $(1 - 2\lambda)$ and $\sum_x \sum_a \phi_{x,a}^4$ the factor $\mu = \frac{N+2}{3}\lambda$ in front, a rescaling of the field ϕ_x is needed to match with the Hamiltonian

$$\mathcal{H}(\{\phi\}) = -\tilde{\beta} \sum_{\langle xy \rangle} \phi_x \phi_y + \sum_x \left[\phi_x^2 + \tilde{\lambda}(\phi_x^2 - 1)^2 \right], \qquad (5)$$

considered, for example, in Ref. [14], where ϕ_x is a real number. We arrive at the equations

$$(1 - 2\lambda) = (1 - 2\tilde{\lambda}) c, \qquad \frac{N+2}{3}\lambda = \tilde{\lambda} c^2 \qquad (6)$$

and hence

$$\frac{6}{N+2}\tilde{\lambda} c^2 + (1 - 2\tilde{\lambda}) c - 1 = 0 \qquad (7)$$

with the solutions

$$c = \frac{-(1 - 2\tilde{\lambda}) \pm \sqrt{(1 - 2\tilde{\lambda})^2 + \frac{24}{N+2}\tilde{\lambda}}}{\frac{12}{N+2}\tilde{\lambda}}, \qquad (8)$$

where we take the positive solution. Plugging in $\tilde{\lambda}^* = 1.1(1)$ [14] we arrive at $c = 1.436(15)$ for $N = 3$. Note that $\tilde{\lambda}^*$ denotes the value of $\tilde{\lambda}$, where leading corrections to scaling vanish. Hence, we get for the improved decoupled model $\lambda_{DI}^* = 1.36(15)$ and $\mu_{DI}^* = \frac{N+2}{3}\lambda_{DI}^* = 2.27(25)$.

B. The observables and dimensionless quantities

Dimensionless quantities or phenomenological couplings play a central role in finite-size scaling. Similar to the study

of O(N)-symmetric models, we study the Binder cumulant U_4, the ratio of partition functions Z_a/Z_p, and the second moment correlation length over the linear lattice size $\xi_{2\text{nd}}/L$. Let us briefly recall the definitions of the observables and dimensionless quantities that we measure.

The energy of a given field configuration is defined as

$$E = \sum_{\langle xy \rangle} \vec{\phi}_x \cdot \vec{\phi}_y . \tag{9}$$

The magnetic susceptibility χ and the second moment correlation length $\xi_{2\text{nd}}$ are defined as

$$\chi \equiv \frac{1}{V} \left\langle \left(\sum_x \vec{\phi}_x \right)^2 \right\rangle , \tag{10}$$

where $V = L^3$ and

$$\xi_{2\text{nd}} \equiv \sqrt{\frac{\chi/F - 1}{4 \sin^2 \pi/L}} , \tag{11}$$

where

$$F \equiv \frac{1}{V} \left\langle \left| \sum_x \exp\left(i \frac{2\pi x_k}{L} \right) \vec{\phi}_x \right|^2 \right\rangle \tag{12}$$

is the Fourier transform of the correlation function at the lowest nonzero momentum. In our simulations, we have measured F for the three directions $k = 0, 1, 2$ and have averaged these three results.

The Binder cumulant U_4 is given by

$$U_4 \equiv \frac{\langle (\vec{m}^2)^2 \rangle}{\langle \vec{m}^2 \rangle^2} , \tag{13}$$

where $\vec{m} = \frac{1}{V} \sum_x \vec{\phi}_x$ is the magnetization of a given field configuration. We also consider the ratio $R_Z \equiv Z_a/Z_p$ of the partition function Z_a of a system with antiperiodic boundary conditions in one of the three directions and the partition function Z_p of a system with periodic boundary conditions in all directions. This quantity is computed by using the cluster algorithm. For a discussion, see Appendix A 2 of Ref. [15].

In order to detect the effect of the cubic anisotropy we study

$$U_C = \frac{\langle \sum_a Q_{4,aaaa}(\vec{m}) \rangle}{\langle \vec{m}^2 \rangle^2} . \tag{14}$$

In the following we shall refer to the dimensionless quantities U_C, U_4, Z_a/Z_p, and $\xi_{2\text{nd}}/L$ by using the symbol R. Note that $U_C = O(\mu)$, while $R = R|_{\mu=0} + O(\mu^2)$ for U_4, Z_a/Z_p, and $\xi_{2\text{nd}}/L$.

In our analysis we need the observables as a function of β in some neighborhood of the simulation point β_s. To this end we have computed the coefficients of the Taylor expansion of the observables up to the third order.

C. Dimensionless quantities for the decoupled system and the first-order transition

In the case of decoupled one-component systems $\lambda - \frac{N+2}{3}\mu = 0$, we can express the dimensionless quantities introduced above in terms of their one-component counterparts.

For example,

$$U_{C,\text{DI}} = \frac{N-1}{N(N+2)}(U_{4,\text{Ising}} - 3) , \tag{15}$$

where $U_{4,\text{Ising}}$ is the Binder cumulant of the one-component system. The calculation is straightforward, only exploiting that $\langle m_a^2 m_b^2 \rangle = \langle m_a^2 \rangle \langle m_b^2 \rangle$ for $a \neq b$ for the decoupled case. Hence, we get for the fixed-point value, which is indicated by an asterisk,

$$U_{C,\text{DI}}^* = [1.603\,59(4) - 3]\frac{N-1}{N(N+2)}$$

$$= -1.396\,41(4)\frac{N-1}{N(N+2)} \tag{16}$$

using the result of [16] for $U_{4,\text{Ising}}^*$. Furthermore, $(Z_a/Z_p)_{\text{DI}} = [(Z_a/Z_p)_{\text{Ising}}]^N$, $U_{4,\text{DI}} = \frac{1}{N} U_{4,\text{Ising}} + \frac{N-1}{N}$, and $(\xi_{2\text{nd}}/L)_{\text{DI}} = (\xi_{2\text{nd}}/L)_{\text{Ising}}$, where the subscripts DI and Ising indicate the decoupled and the one-component system, respectively.

For the first-order transition, in the large-L limit, at the transition temperature, there is the disordered high-temperature phase and the $2N$-fold degenerate ordered phase. Each phase enters with the same weight [17]. In the high-temperature phase, the magnetization vanishes, while for the ordered phase there is a finite magnetization with the modulus m_{order}. Fluctuations of the magnetization vanish as the lattice size is increased. Hence, $\langle \vec{m}^2 \rangle = \frac{0 + 2N m_{\text{order}}^2}{1 + 2N} = \frac{2N}{1+2N} m_{\text{order}}^2$, $\langle (\vec{m}^2)^2 \rangle = \frac{0 + 2N m_{\text{order}}^4}{1 + 2N} = \frac{2N}{1+2N} m_{\text{order}}^4$, and $\langle \sum_a m_a^4 \rangle = \frac{0 + 2N m_{\text{order}}^4}{1+2N} = \frac{2N}{1+2N} m_{\text{order}}^4$. Putting things together we get $U_4 = \frac{2N+1}{2N}$ and $U_C = \frac{(2N+1)(N-1)}{(2N)(N+2)}$. The ratio of partition functions assumes the value $Z_a/Z_p = 0$ and $Z_a/Z_p = 1$ in the limit $L \to \infty$ in the low- and the high-temperature phase, respectively. Taking into account the degeneracy of the ordered phase, we arrive at $Z_a/Z_p = 1/(2N+1)$.

III. FINITE-SIZE SCALING STUDY OF THE RG FLOW: THEORY

Let us outline the general strategy of our analysis and discuss how it arises from the renormalization group theory. Our theoretical framework is the real-space RG as it is discussed, for example, in Ref. [18]. Furthermore, we assume that the picture that arises from the field-theoretic analysis [8] is qualitatively correct.

The key assumption of finite-size scaling is that the RG flow is essentially unaffected by the finiteness of the system, until a scale close to the linear system size L is reached. Furthermore, the dimensionless quantities considered here are invariant under RG transformations. Let us briefly discuss this point for the cumulants U_4 and U_C. Both are constructed from the magnetization $\vec{m} = \frac{1}{V} \sum_x \vec{\phi}_x$. The linear block-spin transformation is considered as a viable RG transformation. It is given by

$$\vec{\Phi}_X = \frac{1}{b^{d-\Delta}} \sum_{x \in X} \vec{\phi}_x , \tag{17}$$

where b, for example $b = 2$, is the linear size of a b^d block. The sites of the coarse lattice are denoted by X and are

identified with blocks on the fine lattice. The field on the coarse lattice is denoted by $\vec{\Phi}_X$. The dimension of the field Δ is *a priori* unknown. Under the transformation (17), the magnetization of a configuration remains exactly the same up to the normalization $1/b^{d-\Delta}$. The cumulants U_4 and U_C are constructed such that this normalization cancels. Hence, U_4 and U_C are exactly invariant under the linear block-spin transformation. For other types of RG transformations this might be only approximately true. Therefore, we expect that U_4 and U_C are affected by corrections related with the redundant RG eigenvalues of the linear block-spin transformation. The leading one can be identified with the analytic background of the magnetic susceptibility. In contrast, the ratio of partition functions Z_a/Z_p should not be affected by such corrections since partition functions stay invariant under any type of RG transformation. This is the reason why below we give preference to Z_a/Z_p, when Z_a/Z_p or $\xi_{2\text{nd}}/L$ could be used.

Typically, we study models with a few parameters: here β, λ, and μ. The RG flow starts with these parameters. Real-space RG transformations generate an infinite number of couplings K_α already in the first step. An important feature of the RG flow is that it rapidly collapses onto low-dimensional submanifolds. In the literature, mostly the collapse onto a fixed point is discussed. For our purpose, this has to be generalized. The RG flow collapses onto lower and lower-dimensional submanifolds in a hierarchical manner. In the neighborhood of fixed points, this hierarchy is given by the values of irrelevant RG eigenvalues y_i. In our problem, as seen in the analysis of the six-loop ϵ expansion [8], we have a rapid collapse on a line in coupling space. The RG flow on this line is slow, corresponding to RG eigenvalues $y \approx 0$ at the fixed points. Note that it is assumed that we are on the critical surface.

In our numerical study, we do not compute the RG flow in terms of couplings K_α. Instead, we monitor the RG flow by studying the behavior of dimensionless quantities R_i. Based on the invariance of dimensionless quantities under RG transformations we might write them as a function of the transformed couplings at the scale of the linear lattice size L:

$$R(L, \beta, \lambda, \mu) = \hat{R}(\vec{K}(L, \beta, \lambda, \mu)), \qquad (18)$$

where the hat indicates that R and $\hat{R}$ are mathematically different functions. The argument of $\hat{R}$ is defined as follows: The RG transformations start with our lattice model at (β, λ, μ). Then n block-spin transformations are performed, such that $L = b^n$. The result of these n transformations is $\vec{K}(L, \beta, \lambda, \mu)$. For sufficiently large L, the RG flow collapses on a line, up to small corrections. Therefore, we might write

$$\hat{R}(\vec{K}(L, \beta = \beta_c, \lambda, \mu)) = \tilde{R}(\tilde{v}(L, \beta = \beta_c, \lambda, \mu)). \qquad (19)$$

We explicitly indicate that we are on the critical surface by setting $\beta = \beta_c$ and the real $\tilde{v}$ parametrizes the line of the slow flow. $\tilde{v}$ should be an analytic function of $\vec{K}$ and $\tilde{v}(L, \beta = \beta_c, \lambda, \mu) = O(\mu)$. These requirements are actually fulfilled by the dimensionless quantity U_C, which we consider as coupling in the following. Roughly speaking, the physics at large scales depends only on the strength of the breaking of the O(N) symmetry, and this strength can be monitored by using U_C. Note, to avoid confusion later on, that U_C has the opposite sign as μ. Our approach is inspired by Ref. [19], where the

dimensionless quantity $\xi(L)/L$ is considered as coupling in an asymptotically free theory. In Ref. [19] a lattice of the size $L \times \infty$ is considered and $\xi(L)$ is the exponential correlation length. For a complementary point of view, see Ref. [20]. Similar to Ref. [19], an RG transformation by the scale factor b is given by

$$U'_C(L, \beta = \beta_c, \lambda, \mu) = U_C(bL, \beta = \beta_c, \lambda, \mu) \qquad (20)$$

for large L. The fixed points are as follows: For O(N) symmetry, at $\mu = 0$, $U'_C = U_C = 0$, at the cubic fixed point $U'_C = U_C = U^*_C$, which we compute below, and at the decoupled Ising fixed point $U'_C = U_C = U^*_{C,\text{DI}}$ [Eq. (16)]. Furthermore, for dimensionless quantities R different from U_C,

$$R(L, \beta = \beta_c, \lambda, \mu) = \tilde{R}(U_C(L, \beta = \beta_c, \lambda, \mu)) \qquad (21)$$

for large L. The large L or scaling limit is obtained by approaching the unstable fixed points, keeping U_C fixed. At the O(N)-invariant fixed point this means that we have to take the limit $L \to \infty$ and $\mu \to 0$ simultaneously, such that U_C stays fixed. The analysis of the six-loop ϵ expansion [8] suggests that the collapse of the RG flow on a single line still occurs far off from the fixed points. Therefore, in our numerical study we expect to see a good approximation of the scaling limit already for moderately large L, while μ is still quite different from zero.

In our numerical study, we compute the RG transformation (20) for finite b. For convenience, we view this as a finite-difference approximation of a β function, where infinitesimal changes of $\ln L$ are considered:

$$\tilde{u}(U_C) = \frac{dU_C}{d\ln L} \approx \frac{U_C(bL) - U_C(L)}{\ln(bL) - \ln L} = \frac{U_C(bL) - U_C(L)}{\ln b}. \qquad (22)$$

At least for U_C not too large, the RG flow is slow and well behaved. Therefore, this should be a good approximation.

In our study we investigate the flow in the whole range of interest. On the one hand we start at the decoupled Ising fixed point. The value $U^*_{C,\text{DI}}$ can be expressed in terms of U^*_4 of the Ising universality class, which is known to high precision [16]. The relevant RG exponent at this fixed point can be expressed in terms of the thermal RG exponent of the Ising universality class [21,22]. The flow runs towards the cubic fixed point. This part of the study can be seen as a benchmark of our approach. Then there is the crossover from the O(N)-symmetric fixed point to the cubic fixed point. Our main focus is on the flow away from the O(N)-symmetric fixed point, towards increasing values of U_C, with a first-order phase transition of increasing strength.

Simulating at a given pair (λ, μ) we can follow the RG flow by simply increasing the lattice size L. However, since the RG flow is slow, only a small range in U_C can be accessed this way. In order to study the whole range, simulations for many different pairs (λ, μ) have to be performed. The results of these simulations are patched together. For moderate sizes of $|U_C|$ this is done by fitting the numerical estimates of $u = \frac{1}{U_C}\tilde{u}$ by using a polynomial *Ansatz*. Note that the zero of $\tilde{u}$ at $U_C = 0$ is lifted in u. The larger $U_C > 0$, the worse is approximation (22) and also fitting u by using a polynomial *Ansatz* requires more and more orders. Therefore, for larger U_C, the patching is done more directly by matching the linear

lattice sizes for two pairs of (λ, μ) such that the estimates of U_C fall on top of each other:

$$U_C(L, \beta = \beta_c, \lambda_1, \mu_1) = U_C(c_{1,2}L, \beta = \beta_c, \lambda_2, \mu_2). \quad (23)$$

For $\mu_1, \mu_2 < 0$, we can not expect that there is a $L \to \infty$ limit of $c_{1,2}$ since eventually we see the first-order phase transition. However, we get estimates of $c_{1,2}$ that are consistent at the level of our numerical precision for some range in L.

Let us summarize the objectives of the study:

(i) Numerically check that the RG flow collapses on a line by, for example, verifying Eq. (21). This done in Sec. IV B.

(ii) Numerically determine the β function, Eq. (22). Based on this we compute the fixed-point value U_C^* at the cubic fixed point, the RG exponent Y_4 at the O(3)-symmetric fixed point, and the correction exponent ω_2 at the cubic fixed point. Note that the exponents are obtained from the derivative of the β function at the fixed points with respect to U_C. This is done in Sec. IV B.

(iii) Motivated by Ref. [8] we compute in Sec. V effective critical exponents as a function of U_C. This is done by using finite-size scaling, and as a check by using the scaling of the correlation length in the thermodynamic limit.

(iv) Finally, in Sec. VI we demonstrate explicitly the first-order nature of the transition for $\mu < 0$ and $|\mu|$ sufficiently large. In particular, we compute the correlation length ξ_{high} in the high-temperature phase at the transition temperature in the thermodynamic limit with high accuracy. Based on the scaling *Ansatz*

$$\xi_{high}(\beta = \beta_c, \lambda, \mu) = \hat{\xi}_{high}(U_C(L, \beta = \beta_c, \lambda, \mu)) L \quad (24)$$

we obtain ξ_{high} for (λ, μ), where we can not simulate lattices with $L \gg \xi_{high}$, which is required to get a good approximation of the thermodynamic limit, using our limited computational resources. Here we denote, a bit sloppy, the inverse transition temperature by β_c. In the spirit of Ref. [20], by using $\xi_{high}(\lambda_2, \mu_2) = c_{1,2}\xi_{high}(\lambda_1, \mu_1)$, we obtain iteratively results for weaker and weaker transitions, where the factor $c_{1,2}$ is given by Eq. (23). The latter is already done in Sec. IV B using results obtained in Sec. VI.

IV. FINITE-SIZE SCALING STUDY OF THE RG FLOW: NUMERICS

As first step of our numerical study, we repeat the analysis of Sec. VII of Ref. [6] with more data. We have added new pairs of (λ, μ), in particular, for relatively large values of $|\mu|$. Furthermore, for pairs (λ, μ) already studied in Ref. [6] we improved the statistics and added larger lattice sizes. As a preliminary step, generalizing the idea of improved models, we locate the line of slow flow in the (λ, μ) plane. Then we continue with the study of the flow of U_C as outlined in the previous section. Note that in Appendix A we collect some technical aspects of the numerical analysis and discuss how we arrive at final results.

A. Locating the line of slow RG flow in the (λ, μ) plane

In the study of critical phenomena by using lattice models, improved models have been demonstrated to be helpful in obtaining accurate estimates of universal quantities. For a

discussion, see, for example, Sec. 2.3 of Ref. [1]. In the case of the Heisenberg universality class, improved models had been studied, for example, in Refs. [5,12,23]. The basic idea is that a parameter of the model is tuned such that the scaling field of the leading correction to scaling vanishes. In the case of the three-component ϕ^4 model, Eq. (3) with $\mu = 0$, this is achieved for $\lambda^* = 5.17(11)$ (see Ref. [23]). In Ref. [6], we have applied the idea to the cubic fixed point, now eliminating the scaling fields of the two leading corrections. For $N = 3$, we get $(\lambda, \mu)^*_{cubic} = (4.99(11), 0.28(2))$. Above in Sec. II, we have already discussed how the result [14] for the one-component ϕ^4 model translates to the decoupled ϕ^4 case. In the case of the O(3)-symmetric ϕ^4 model, we have analyzed our data for dimensionless quantities by using *Ansätze* of the form

$$R_i(\beta_c, \lambda, L) = R_i^* + r_i w(\lambda) L^{-\omega} + \cdots, \quad (25)$$

where λ^* is obtained as zero of $w(\lambda)$. In Ref. [6], Eq. (66), we have generalized Eq. (25) to the line of slow flow that we eventually intend to study:

$$R_i(\beta_c, \lambda, \mu, L) = R_i^* + \sum_{m=2}^{m_{max}} c_{i,m} U_C^m(\beta_c, \lambda, \mu, L)$$
$$+ r_i w(\lambda, \mu) L^{-\omega} + \sum_j a_{i,j} L^{-\epsilon_j} \quad (26)$$

for dimensionless quantities that behave like $R_i(\beta_c, \lambda, \mu, L) = R_i(\beta_c, \lambda, 0, L) + O(\mu^2)$. The $O(\mu^2)$ contributions are taken into account by the term $\sum_{m=2}^{m_{max}} c_{i,m} U_C^m(\beta_c, \lambda, \mu, L)$. In fact, we perform a Taylor expansion of Eq. (21). Note that we obtain dimensionless quantities $R_i - \sum_{m=2}^{m_{max}} c_{i,m} U_C^m$ that, at least approximately, remain invariant under the slow part of the RG flow. Corrections are assumed to be of the same form as corrections to scaling in the neighborhood of a fixed point. Furthermore, the exponent ω is assumed to be constant, taking the value $\omega = 0.759(2)$ of the Heisenberg universality class [23]. This is motivated by the fact that ω_1 of the cubic universality class differs by little from ω of the Heisenberg one. Furthermore, ω of the Ising universality class, which is the correction exponent at the decoupled Ising fixed point, is only slightly larger than the correction exponent of the Heisenberg universality class. In our fits we set $r_{U_4} = 1$, while r_{Z_a/Z_p} and $r_{\xi_{2nd}/L}$ are free parameters. Terms proportional to $L^{-2\omega}$ and higher are not taken into account since for our data the correction is small. The last term of Eq. (26) takes into account subleading corrections with $\epsilon_j \gtrsim 2$. Also, these correction exponents are assumed to be constant. In the fits performed here, we took two exponents $\epsilon_1 = 2 - \eta$ and $\epsilon_2 = 2.023$, corresponding to the analytic background of the magnetization and the breaking of the rotational invariance by the lattice. In the case of the analytic background, we assume that the coefficients depend linearly on λ and quadratically on μ. The coefficients for the breaking of the rotational invariance are taken as a constant. Formally, in Eq. (26), the correction term $r_i w(\lambda, \mu) L^{-\omega}$ is of the same type as those contained in $\sum_j a_{i,j} L^{-\epsilon_j}$. We single out the term with the smallest correction exponent since in the following we like to focus on (λ, μ), where $w(\lambda, \mu) \approx 0$, which defines the line of the slow flow in the (λ, μ) plane.

The *Ansatz* (26) is used for joint fits of Z_a/Z_p, ξ_{2nd}/L, and U_4. In a first series of fits, we took $w(\lambda, \mu)$ as a free parameter for each value of (λ, μ). We performed a number of fits, varying the range of μ that is taken into account, the maximal power m_{max} of U_C and, as usual, the minimal linear lattice size L_{min} taken into account. The different sets of data that we analyzed are mainly characterized by the range of μ that is taken. For the smallest set of data, $|\mu| \leqslant 1.2$ is taken, while for the largest $-1.8 \leqslant \mu \leqslant 2.2$ is taken. The largest set contains 64 different pairs of (λ, μ). For negative μ we used the additional cut $U_C \lesssim 0.4$. As a result, for $(\lambda, \mu) = (3.4, -1.8)$, $(3.0, -1.663)$, and $(2.7, -1.552)$ only linear lattice sizes up to $L = 48$ are used in the fit.

In the case of our largest data set, we performed fits with $m_{max} \leqslant 9$. For $m_{max} = 9$, we get $\chi^2/\text{DOF} = 1.070$, 1.045, and 1.002, corresponding to $p = 0.049$, 0.154, and 0.478 for $L_{min} = 20$, 24, and 28, respectively. For the definitions of χ^2/DOF and the p value see Appendix A. For smaller ranges of μ, acceptable fits were obtained already for smaller L_{min}. For example, for $L_{min} = 16$, $|\mu| \leqslant 1.2$, and $m_{max} = 6$ we get $\chi^2/\text{DOF} = 1.052$, corresponding to $p = 0.103$. Note that in Ref. [6] we have used $m_{max} = 5$ at most and fitted data for $|\mu| \leqslant 1$.

Next we used the parametrizations

$$w(\lambda, \mu) = a(\lambda - \lambda^* - c\mu^2 - d\mu^3) \, [1 + e(\lambda - 5.0)] \quad (27)$$

and

$$w(\lambda, \mu) = a(\lambda - \lambda^* - c\mu^2 - d\mu^3 - e\mu^4) \, [1 + f(\lambda - 5.0)]$$
$$(28)$$

for the correction amplitude.

Here acceptable fits were only obtained for data sets with a range up to $1.5 \geqslant \mu \geqslant -1.566$. Various acceptable fits, using Eq. (28), are consistent with the estimates $\lambda^* = 5.12(5)$, $c = -0.8(1)$, $d = 0.06(1)$, and $e = 0.01(4)$ for the line of slow flow.

In Fig. 1 we plot the line of slow flow as characterized by Eq. (28) with the numerical values of the parameters given above. In addition we plot the pairs of (λ, μ) we have simulated at. The pairs of (λ, μ) with a small correction amplitude w are shown as solid circles. Here, small means that it fits without parametrization of w, the modulus of the value of w is at most a few times the error of w. The improved point of the decoupled Ising system is obtained from $\tilde{\lambda}^* = 1.1(1)$ for the one-component ϕ^4 model on the simple cubic lattice [14] as discussed in Sec. II. Finally, the pairs of (λ, μ), where, below in Sec. VI, we demonstrate directly that the transition is first order, are plotted.

Our results for the dimensionless quantities are fully consistent with those obtained in Ref. [6]. The estimates of $c_{i,m}$, summarized in Table I, are more accurate now. The error bars are taken such that the results of five different acceptable fits are covered. We give results up to $m = 4$. For larger m, the values of $c_{i,m}$ differ substantially between different fits.
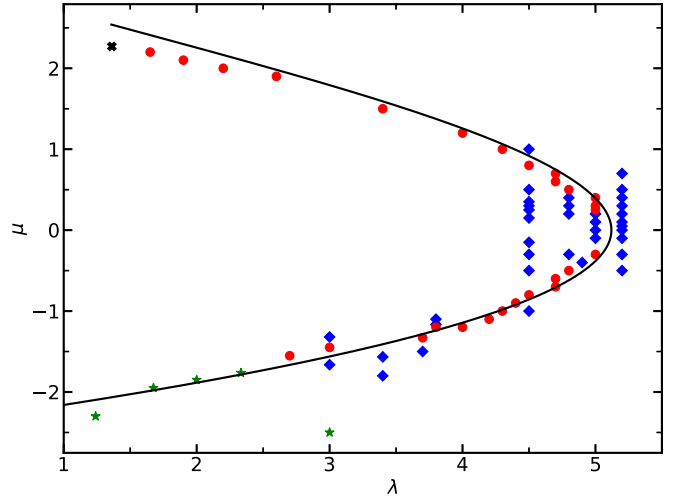

FIG. 1. We plot the line of slow flow in the (λ, μ) plane as parametrized by Eq. (28) using the numerical values $\lambda^* = 5.12$, $c = -0.8$, $d = 0.06$, and $e = 0.01$ as solid black line. The solid circles give values of (λ, μ) with a small correction amplitude w. These are used in the analysis of the RG flow below. Additional pairs of (λ, μ) that are analyzed in this section are plotted as diamonds. The cross gives the improved point for the decoupled Ising system. The asterisks give points, where, below in Sec. VI, we demonstrate directly that the transition is first order.

Selected estimates of the inverse transition temperature β_c are provided as Supplemental Material [24].

B. Flow equation for U_C

Now we proceed with the analysis of the RG flow, as outlined in Sec. III. We like to study the RG flow on the critical surface. To this end, following Ref. [25], we take the quantities of interest at $\beta = \beta_f$, where a dimensionless quantity R_i, different from U_C, assumes a certain value $R_{i,f}: R_i(\beta_f) = R_{i,f}$. Quantities taken at β_f are indicated by a line on top. For example, U_C at β_f is denoted by $\overline{U}_C$ in the following. Replacing a numerical estimate of β_c by β_f has various advantages. For example, the statistical error is typically reduced due to cross correlations with R_i (see, for example, Ref. [26]). Following previous work, for example, [12,14,15,23], we take the ratio of partition functions Z_a/Z_p to define β_f. Our choice for the fixed value is $(Z_a/Z_p)_f = 0.194\,77$, which is the estimate of the fixed-point value for the Heisenberg universality class [23]. Note that for any value of $R_{i,f}$ in the range of R_i, for a second-order phase transition, β_f converges to β_c as the linear

TABLE I. Estimates of the coefficients $c_{i,m}$ [Eq. (26)] for the three dimensionless quantities that we have analyzed. For a discussion, see the text.

$R_i \setminus m$	2	3	4
Z_a/Z_p	$-0.612(9)$	$2.13(8)$	$-5.0(1.2)$
ξ_{2nd}/L	$1.308(9)$	$-3.38(7)$	$11.7(9)$
U_4	$1.243(8)$	$-2.73(6)$	$8.6(1.4)$

lattice size L increases. For $R_{i,f} = R_i^*$ the convergence is the fastest.

Motivated by the results of the previous subsection, we consider as alternative

$$(Z_a/Z_p)(\beta_f) - \sum_{j=2}^{m_{max}} c_{Z_a/Z_p,j} U_C^j(\beta_f) = 0.194\,77, \qquad (29)$$

where $c_{Z_a/Z_p,j}$ and m_{max} are fixed. The idea of using Eq. (29) is that, in particular for large values of $|U_C|$, the convergence of β_f with increasing L is improved by using a quantity that is approximately invariant under the RG flow. In our numerical analysis we use $m_{max} = 6$. The values $c_{Z_a/Z_p,2} = -0.61$ and $c_{Z_a/Z_p,3} = 2.1$ are taken from the fits discussed above, while $c_{Z_a/Z_p,4} = -2.9$, $c_{Z_a/Z_p,5} = -10$, and $c_{Z_a/Z_p,6} = 20.8$ are chosen such that for large $|U_C|$ certain requirements to be discussed below are fulfilled. We do not simply use numerical results of $c_{Z_a/Z_p,j}$ for $j > 3$, obtained by the fits performed in the previous section, since for U_C outside of the range of these fits the invariance under the RG flow is rapidly lost. Instead, the coefficients are chosen such that the decoupled Ising fixed point and the first-order transition on the other side are approached properly.

To this end, let us view

$$(Z_a/Z_p)_{\text{mod},f}(U_C) = \sum_{j=2}^{m_{max}} c_{Z_a/Z_p,j} U_C^j + (Z_a/Z_p)_f \qquad (30)$$

as a function of U_C. The coefficients $c_{Z_a/Z_p,4}$, $c_{Z_a/Z_p,5}$, and $c_{Z_a/Z_p,6}$ in Eq. (29) are chosen such that $(Z_a/Z_p)_{\text{mod},f}(U_C)$

(i) is monotonically decreasing with increasing U_C in the range $0 < U_C \lessgtr 0.4$;

(ii) assumes roughly the numerical value found for Z_a/Z_p at the transition temperature for $U_C \approx 0.4$;

(iii) is monotonically decreasing with decreasing U_C in the range $0 > U_C \geqslant U_{C,\text{DI}}$;

(iv) assumes the decoupled Ising value of Z_a/Z_p for $U_{C,\text{DI}}$.

One should note that the numerical results discussed below in Sec. VI show that at the inverse transition temperature β_t, with increasing linear lattice size L, the limiting values of the dimensionless quantities are not approached monotonically. For example, one finds the extrema $(Z_a/Z_p)_{min} \approx 0.131$ and $U_{C,max} \approx 0.504$, both at $L/\xi_{\text{high}} \approx 2$, consistently for different values of ξ_{high}. Plugging in $N = 3$ into the equations of Sec. II C, we get $Z_a/Z_p = \frac{1}{7} = 0.142\,857\ldots$ and $U_C = 0.466\,666\ldots$ in the large-L limit. Studying the flow of $\overline{U}_C$, we stay in the range of L, where it is monotonic.

We performed the following analysis for both choices $(Z_a/Z_p)_f = 0.194\,77$ and Eq. (29). We obtain consistent results for these two choices. It is assuring that the results virtually do not depend on the choices, partly made *ad hoc*, when fixing $c_{Z_a/Z_p,j}$ in Eq. (29). Not to overburden the reader, in the discussion below we only present the results obtained by using Eq. (29). In order to keep corrections to scaling small, we focus on data obtained for (λ, μ) close to the line of slow flow as discussed above in Sec. IV A.

In order to check Eq. (21), we plot $\overline{U}_4$ versus $\overline{U}_C$ for six pairs of (λ, μ) in Fig. 2. For $(2.333, -1.764)$ and $(2.0, -1.85)$, we show in Sec. VI that the transition is of first order. The data points for the different pairs of
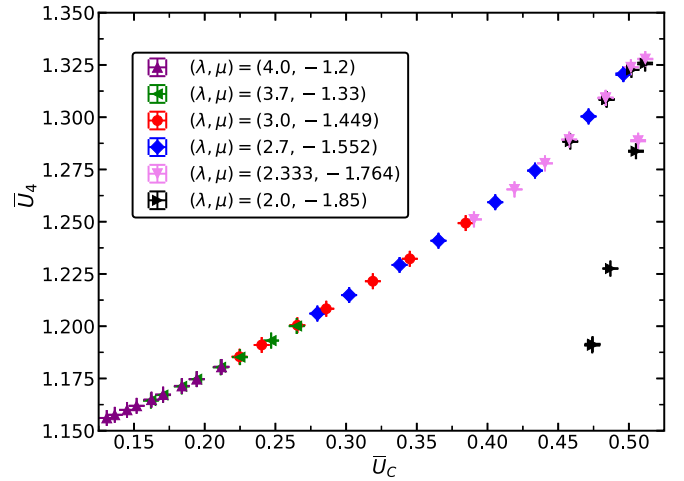

FIG. 2. We plot $\overline{U}_4$ versus $\overline{U}_C$ obtained for six different pairs of (λ, μ) and a number of linear lattice sizes $L \geqslant 12$. The largest lattice size is $L = 192, 128, 96, 128, 64$, and 48 for $(\lambda, \mu) = (4.0, -1.2)$, $(3.7, -1.33)$, $(3.0, -1.449)$, $(2.7, -1.552)$, $(2.333, -1.764)$, and $(2.0, -1.85)$, respectively. For a discussion see the text.

(λ, μ) fall nicely on a single curve, confirming that there is a single-parameter RG flow, which is reached to a good approximation for the linear lattice sizes $L \geqslant 12$ studied here. For $(2.333, -1.764)$ and $(2.0, -1.85)$ we see a second branch of the curve, which is due to the nonmonotonic behavior discussed above. Even here the data for $(\lambda, \mu) = (2.333, -1.764)$ and $(2.0, -1.85)$ seem to fall on top of each other.

The flow of $\overline{U}_C$ is characterized by

$$u(\overline{U}_C) = \frac{1}{\overline{U}_C} \frac{d\overline{U}_C}{d \ln L}, \qquad (31)$$

where we have introduced the factor $\frac{1}{\overline{U}_C}$, compared with a β function in field theory, for numerical convenience. The factor lifts the zero of the β function at $\overline{U}_C = 0$. Note that here we replace $U_C(L, \beta = \beta_c, \lambda, \mu)$ of Sec. III by $U_C(L, \beta = \beta_f, \lambda, \mu)$. Let us first discuss the behavior of u in the neighborhood of the decoupled Ising fixed point. The decoupled Ising fixed point is unstable with an RG exponent

$$y = \alpha_I y_{t,I} = 2y_{t,I} - d = d - 2\Delta_{\epsilon,I} = 0.174\,75(2), \quad (32)$$

where α_I and $y_{t,I}$ are the specific heat and the thermal RG exponent of the three-dimensional Ising universality class, respectively [21,22]. The numerical value of the scaling dimension $\Delta_\epsilon = 1.412\,625(10)$ is taken from Ref. [27]. In the neighborhood of the decoupled Ising fixed point we have

$$\overline{U}_C(L) = \overline{U}_{C,\text{DI}} + \epsilon_0 (L/L_0)^y + \cdots. \qquad (33)$$

Hence,

$$u(\overline{U}_{C,\text{DI}} + \epsilon_0) \approx \overline{U}_{C,\text{DI}}^{-1} \lim_{L \to L_0} \frac{\epsilon_0 (L/L_0)^y - \epsilon_0}{\Delta \ln L}$$

$$= \overline{U}_{C,\text{DI}}^{-1} \lim_{L \to L_0} \frac{\epsilon_0 y \Delta \ln L}{\Delta \ln L} = \overline{U}_{C,\text{DI}}^{-1} \epsilon_0 y, \quad (34)$$

where $\Delta \ln L = \ln L - \ln L_0 = \ln(L/L_0)$. Furthermore, we have used $(L/L_0)^y = \exp[y \ln(L/L_0)] = 1 + y \ln(L/L_0) + \cdots$.

In Ref. [6] we estimated u, Eq. (31), by fitting data for fixed (λ, μ) by using the *Ansatz*

$$\overline{U}_C(\lambda, \mu, L) = aL^u \qquad (35)$$

or as check

$$\overline{U}_C(\lambda, \mu, L) = aL^u \, (1 + cL^{-2}) \qquad (36)$$

for some range $L_{\min} \leqslant L \leqslant L_{\max}$. As argument of u we took $[\overline{U}_C(L_{\min}) + \overline{U}_C(L_{\max})]/2$. The approximations (35) and (36) rely on the fact that $\overline{U}_C$ varies only little in the range $L_{\min} \leqslant L \leqslant L_{\max}$ and hence u is small:

$$\begin{aligned}
\overline{U}_C(L) &\approx \overline{U}_C(L_0) + \overline{U}_C(L_0) \, u \, \ln(L/L_0) \\
&= \overline{U}_C(L_0) \, [1 + u \ln(L/L_0)] \\
&\approx \overline{U}_C(L_0) \, \exp[u \ln(L/L_0)] \propto L^u,
\end{aligned} \qquad (37)$$

where $L_0 = \sqrt{L_{\min} L_{\max}}$. In Eq. (36), the factor $(1 + cL^{-2})$ is included to take subleading corrections to scaling approximately into account.

For (λ, μ), where $\overline{U}_C$ changes considerably over the range of lattice sizes L that we simulate, we now take instead

$$\begin{aligned}
&u([\overline{U}_C(L_2) + \overline{U}_C(L_1)]/2) \\
&\quad = \frac{2}{\overline{U}_C(L_2) + \overline{U}_C(L_1)} \frac{\overline{U}_C(L_2) - \overline{U}_C(L_1)}{\ln(L_2/L_1)}
\end{aligned} \qquad (38)$$

as approximation. Here L_1 and L_2 are lattice sizes we simulated at and L_2 is the smallest that satisfies $L_2 > L_1$, meaning the next larger to L_1. Note that Eq. (38) is the finite-difference approximation of Eq. (31).

First we check that estimates of u, Eq. (31), obtained for different values of (λ, μ) fall on a unique curve, up to small deviations that can be interpreted as corrections. To this end, we first compare the estimates obtained from two different pairs of (λ, μ) that give approximately the same values of $\overline{U}_C$ for the same lattice size L. The leading correction should differ between these two pairs. In Fig. 3 we plot our estimates of u for $(\lambda, \mu) = (3.4, -1.566)$ and $(3.0, -1.449)$. For example, from the fit with the *Ansatz* (26), taking $m_{\max} = 9$, and our largest set of data, we get for $L_{\min} = 24$ the estimates $w = -0.0038(5)$ and $0.0017(5)$, respectively. In particular, the difference between these two estimates of w is very stable when varying the parameters of the fit. In both cases, estimates of u obtained from the linear lattice sizes $L = 12, 16, 24, 32, 48, 64,$ and 96 are shown. Note that $\overline{U}_C$ is monotonically increasing with the linear lattice size L in the range plotted here. We find that the results obtained for $(L_1, L_2) = (12, 16)$, which is leftmost in the plot, and $(16,24)$ for the two pairs of (λ, μ) clearly differ by more than the statistical error. However, the difference is small compared with the value of u.

Next, in Fig. 4 we plot our estimates of u computed by using Eq. (38) obtained for five different pairs of (λ, μ), which are approximately on the line of slow flow. For small linear lattice sizes, we expect that subleading corrections are numerically dominant corrections. It is quite clear from the
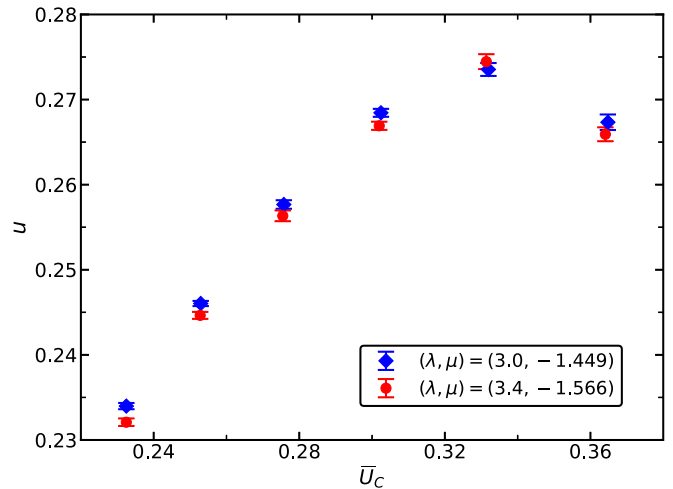

FIG. 3. We plot estimates of u, Eq. (31), computed by using Eq. (38) and the data for $(\lambda, \mu) = (3.4, -1.566)$ and $(3.0, -1.449)$ as a function of $\overline{U}_C$. The data are obtained for the pairs of lattice sizes $(L_1, L_2) = (12, 16), (16, 24), ..., (64,96)$. Since $\overline{U}_C$ increases with L in the given range, the leftmost points correspond to $(L_1, L_2) = (12, 16)$, while the rightmost ones correspond to $(L_1, L_2) = (64, 96)$. For a discussion see the text.

plot that estimates obtained from $(L_1, L_2) = (12, 16)$ are too large compared with the asymptotic value. Note that the data points for $(L_1, L_2) = (12, 16)$ are the leftmost ones for each pair (λ, μ) which is considered. For $(L_1, L_2) = (24, 32)$ the inspection by eye does not show such a deviation, suggesting that corrections to scaling are at most at the level of the statistical error at this point.

In Fig. 5 we plot estimates of u obtained by using Eq. (35) with $L_{\min} = 24$ and Eq. (38) as a function of $\overline{U}_C$. Furthermore, we give $u = 0$ for the decoupled Ising point at $\overline{U}_C = -0.186\,188(5)$ and the behavior of u in the neighborhood of the decoupled Ising point. For $|u| \lessapprox 0.1$ the estimates obtained by using Eqs. (35) and (38) are consistent. For
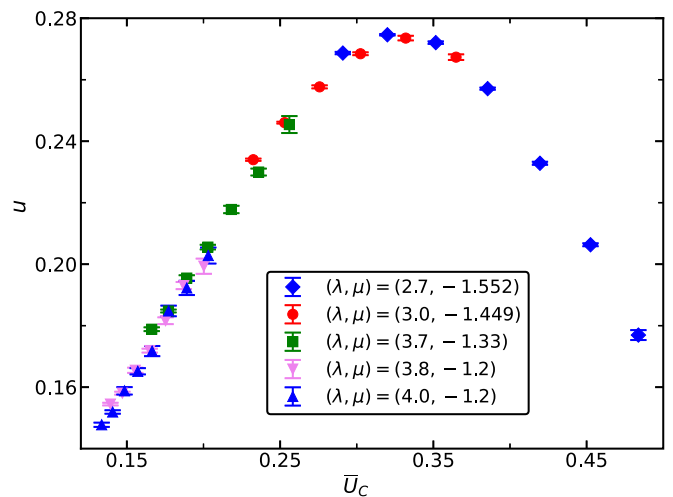

FIG. 4. We plot estimates of u, Eq. (31), computed by using Eq. (38) and the data for $(\lambda, \mu) = (2.7, -1.552)$, $(3.0, -1.449)$, $(3.7, -1.3)$, $(3.8, -1.2)$, and $(4.0, -1.2)$, as a function of $\overline{U}_C$. For a discussion see the text.
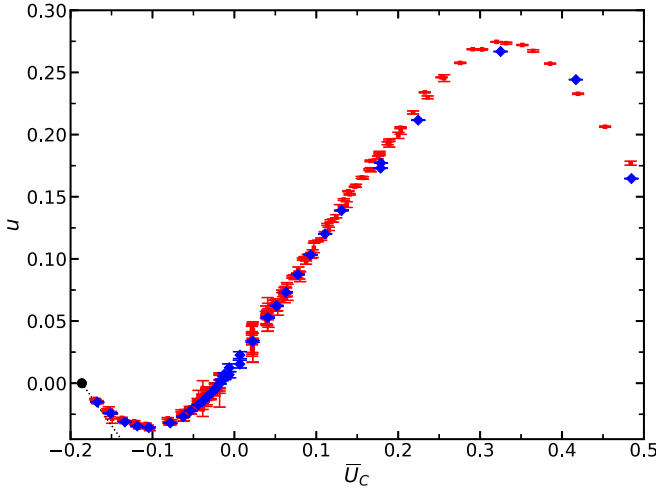
FIG. 5. We plot u, Eq. (31), obtained from a large set of (λ, μ) as a function of $\overline{U}_C$. Results obtained by using Eq. (35) are given as diamonds, while those obtained by using Eq. (38) are given as squares. The filled circle gives the result for the decoupled Ising system. The dotted line shows the behavior (34) in the neighborhood of the decoupled Ising system. Details are discussed in the text.

$u > 0.15$ we see clear differences. For small $|u|$, the statistical error is quite large for Eq. (38). This is partially due to the fact that we simulated for more values of L in the same range of lattice sizes than for larger $|u|$. The behavior for $\overline{U}_C \lesssim -0.15$ seems to be consistent with the predictions for the decoupled Ising system and its neighborhood.

We analyze the numerical results by using the *Ansatz*

$$u = \sum_{i=0}^{n} a_i \overline{U}_C^{\,i}, \tag{39}$$

where we have taken $n = 3$, 4, and 5 in our fits. In Appendix B, we discuss the cases $n = 1$ and 2 analytically. In our preliminary analysis, we experimented with various approaches. For example, we combined data for $|\mu| \leqslant 0.6$ analyzed by using Eq. (35) with data for $|\mu| > 0.6$ analyzed by using Eq. (38).

In our final analysis, we use for simplicity only data with $|\mu| \geqslant 0.6$ analyzed by using Eq. (38). Note that for $(\lambda, \mu) = (4.7, 0.6)$ we have $\overline{U}_C(L) = -0.034\,532(8),...,$ $-0.033\,963(22)$ for $L = 12,...,64$ and for $(\lambda, \mu) = (4.7, -0.6)$ we have $\overline{U}_C(L) = 0.047\,872(7),...,0.053\,152(27)$

for $L = 12,...,64$. In the fit, the covariances that are caused by the fact that the numerical result for $\overline{U}_C(L)$ might appear in two differences, one with a smaller and one with a larger lattice size, are taken into account. In order to estimate the effects of the truncation in Eq. (39) and corrections to scaling, we vary the maximal $|\overline{U}_C|$ and $|\mu|$ and minimal lattice size $L_{1,\min}$ that is taken into account. Our final results are based on four different fits. In the first one, fit 1 in Table II, we included $(\lambda, \mu) = (2.7, -1.552)$, $(3.0, -1.449)$, $(3.7, -1.33)$, $(3.8, -1.2)$, $(4.0, -1.2)$, $(4.2, -1.1)$, $(4.3, -1.0)$, $(4.4, -0.9)$, $(4.5, -0.8)$, $(4.7, -0.7)$, $(4.7, -0.6)$, $(4.7,0.6)$, $(4.7,0.7)$, $(4.5,0.8)$, $(4.3,1.0)$, $(4.0,1.2)$, $(3.4,1.5)$, $(2.6,1.9)$, $(2.2,2.0)$, $(1.9,2.1)$, and $(1.65,2.2)$. In the case of $(\lambda, \mu) = (2.7, -1.552)$ we skipped the lattice sizes $L > 64$ since the value of $\overline{U}_C$ is too large to be fitted with the *Ansatz* (39). Furthermore, we take $n = 5$ in Eq. (39) and $L_{1,\min} = 48$. In the remaining fits, smaller ranges of (λ, μ) are used. The values of (λ, μ) taken into account range from $(3.7, -1.33)$ to $(1.65,2.2)$, $(4.0, -1.2)$ to $(2.2,2.0)$, and $(4.2,1.1)$ to $(2.6,1.9)$ for fits 2, 3, and 4, respectively. Furthermore, the fits 2, 3, and 4 are characterized by $L_{1,\min} = 32$, 24, 24 and $n = 5$, 4, 3, Eq. (39), respectively. In the case of fit 1, $\overline{U}_C$ ranges from $-0.151\,18(7)$ to $0.405\,51(4)$, while for fit 4, it ranges from $-0.106\,242(13)$ to $0.139\,89(7)$. The estimates of the parameters a_i are summarized in Table II. Based on these estimates, we compute $\overline{U}_C^*$, which is the zero of u, numerically. Furthermore, ω_2 is given by minus the derivative of $\tilde{u} = \overline{U}_C u$ with respect to $\overline{U}_C$ at $\overline{U}_C^*$. The statistical errors of these derived quantities are obtained by error propagation as discussed in Appendix A. It turns out that the difference $Y_4 - \omega_2$ has a much smaller statistical error than $Y_4 = a_0$ and ω_2, individually. This can be attributed to a strong statistical correlation of Y_4 and ω_2. The strong correlation is not surprising since for $a_{i\geqslant 2} = 0$ we get $Y_4 = \omega_2$ (see Appendix B). The final results given in Table II and their error bars are chosen such that the results of the four fits discussed above are covered. For a discussion of the error analysis see Appendix A.

As a final check, we repeated the analysis, replacing $(\lambda, \mu) = (3.7, -1.33)$, $(3.8, -1.2)$, $(4.0, -1.2)$, $(4.2, -1.1)$, and $(4.3, -1.0)$ by $(\lambda, \mu) = (3.0, -1.663)$, $(3.4, -1.8)$, $(3.7, -1.5)$, $(4.0, -1.2)$, and $(4.5, -1.0)$. For these values of (λ, μ) the amplitude $|w|$ of corrections is larger than for the replaced ones. The results do not change significantly.

TABLE II. Fitting numerical estimates of u, Eq. (38), by using the *Ansatz* (39). The fits, which are labeled by 1, 2, 3, and 4, are discussed in the text. In addition to the estimates given in the table, we obtain $a_5 = -18.1(2.5)$ and $42.7(9.3)$ for the fits 1 and 2, respectively. We get $\chi^2/\text{DOF} = 0.965, 0.970, 0.934$, and 0.968 corresponding to $p = 0.524, 0.538, 0.623$, and 0.542 for fits 1, 2, 3, and 4, respectively. In the case of the fits 1, 2, 3, and 4 we give statistical errors, while for the final results systematic errors are taken into account, as discussed in Appendix A.

Fit	a_0	a_1	a_2	a_3	a_4	$\overline{U}_C^*$	ω_2	$Y_4 - \omega_2$
1	0.01441(66)	0.8136(72)	2.004(55)	−8.7(4)	12.9(1.9)	−0.0186(8)	0.01360(59)	0.00081(6)
2	0.01348(38)	0.8296(34)	2.398(69)	−10.5(3)	−1.4(2.6)	−0.0172(4)	0.01267(31)	0.00081(3)
3	0.01448(21)	0.8367(25)	2.193(41)	−10.5(2)	10.0(1.9)	−0.0183(3)	0.01362(20)	0.00086(2)
4	0.01401(18)	0.8358(28)	2.357(23)	−10.4(3)		−0.0177(2)	0.01315(16)	0.00086(2)
Final	0.0141(10)	0.823(17)	2.21(26)	−9.6(1.3)		−0.0181(14)	0.0133(9)	0.00081(7)

TABLE III. Results for the scale factor c for the matching between $(\lambda, \mu) = (2.333, -1.764)$ and $(2.7, -1.552)$. L is the linear lattice size for $(\lambda, \mu) = (2.333, -1.764)$ and $c_{1,2}$ gives the ratio with the matching lattice for $(\lambda, \mu) = (2.7, -1.552)$ as defined by Eq. (40). For a discussion see the text.

L	$c_{1,2}$
12	3.4351(35)
16	3.4478(18)
24	3.4558(23)
32	3.4523(44)

C. Matching

For two pairs of parameters (λ_1, μ_1) and (λ_2, μ_2) we determine a scale factor $c_{1,2}$ by requiring that

$$\overline{U}_{C,1}(L) = \overline{U}_{C,2}(c_{1,2}L), \tag{40}$$

where the second subscript indicates the pair of parameters. This is solved numerically for each linear lattice size that we simulated for parameter pair one. In a first step, for $\mu < 0$, we determine two lattice sizes L_1 and L_2 for the second parameter pair such that L_2 is the smallest linear lattice size simulated such that $\overline{U}_{C,1}(L) \leqslant \overline{U}_{C,2}(L_2)$ and L_1 the largest such that $\overline{U}_{C,1}(L) \geqslant \overline{U}_{C,2}(L_1)$. If such a pair of lattice sizes exists, we interpolate $\overline{U}_{C,2}$ linearly in the logarithm of the linear lattice of the second parameter pair. As an example, in Table III, we give the results of the matching for $(\lambda_1, \mu_1) = (2.333, -1.764)$ and $(\lambda_2, \mu_2) = (2.7, -1.552)$. Note that for $(\lambda, \mu) = (2.333, -1.764)$ we find in Sec. VI that $\xi_{high} = 24.70(2)$ at the transition temperature. Furthermore, for $(\lambda, \mu) = (2.333, -1.764)$ we reach linear lattice sizes, where $\overline{U}_C(L)$ becomes nonmonotonic. We get $\overline{U}_C = 0.390\,42(10)$, $0.419\,10(4)$, $0.457\,81(5)$, $0.483\,59(5)$, $0.511\,61(6)$, $0.506\,55(12)$ for $L = 12, 16, 24, 32, 48,$ and 64. The linear lattice sizes given in Table III are still in the range, where $\overline{U}_C(L)$ monotonically increases with the linear lattice size L.

We find that $c_{1,2}$ changes only little with increasing L. It seems plausible that for $L = 32$ systematic errors are at most of the same size as the statistical error given in Table III. To check whether $c_{1,2}$ indeed gives the ratio of the correlation length ξ_{high} at (λ_1, μ_1) and (λ_2, μ_2), we performed the matching for $(\lambda_1, \mu_1) = (2.0, -1.85)$ and $(\lambda_2, \mu_2) = (2.333, -1.764)$. Here we get $c_{1,2} = 2.0165(30)$, $2.0168(14)$, and $2.0139(15)$ for $L = 12, 16,$ and 20, respectively. This can be compared with the ratio $24.70(2)/12.135(6) = 2.0354(19)$ of the correlation length in the high-temperature phase computed in Sec. VI. The correction to the expected scaling is small.

We continued this matching for pairs (λ_1, μ_1) and (λ_2, μ_2) that are approximately on the line of slow flow. In Table IV we report our final results for the matching factor $c_{1,2}$. The error bar includes a rough estimate of the systematic error, obtained from the variation of $c_{1,2}$ with increasing L. Based on our simulations, we can not proceed to $\mu > -1$ since we have no pairs of (λ, μ) at hand that have overlapping ranges of $\overline{U}_C$. In the third column, we give an estimate of the correlation length in the high-temperature phase at the tran-

TABLE IV. Results for the scale factor $c_{1,2}$ for a sequence of pairs of (λ, μ). The pairs (λ, μ) are given in the first column. We match subsequent pairs of (λ, μ). The estimates of $c_{1,2}$ given in the second column refer to (λ_1, μ_1) given one row above, and (λ_2, μ_2) given in the same row. The estimate of ξ_{high} given in the third column is obtained by multiplying up the values for $c_{1,2}$, starting from $\xi_{high} = 24.70(2)$ for the correlation length in the high-temperature phase at the transition temperature at $(\lambda, \mu) = (2.333, -1.764)$. The errors for the correlation length are added up. For a discussion see the text.

(λ, μ)	$c_{1,2}$	ξ_{high}
$(2.333, -1.764)$		24.70(2)
$(2.7, -1.552)$	3.455(7)	85.34(24)
$(3.0, -1.449)$	2.463(10)	210.2(1.4)
$(3.7, -1.33)$	5.31(2)	1116.0(12.0)
$(3.8, -1.2)$	2.99(2)	3337.0(58.0)
$(4.0, -1.2)$	1.33(1)	4438.0(110.0)
$(4.2, -1.1)$	3.35(4)	14870.0(550.0)
$(4.3, -1.0)$	3.6(1)	53500.0(3500.0)

sition temperature. We start from the direct estimate obtained for $(\lambda, \mu) = (2.333, -1.764)$ in Sec. VI. Then we multiply up the values for $c_{1,2}$. The error bar is simply computed by adding up the error due to the previous estimate of ξ_{high} and the one due to the uncertainty of the current value of $c_{1,2}$. This is done since we do not know how the errors are correlated.

Going to $\mu > -1$ we evaluate the RG flow by using Eq. (31). Here we abstain for simplicity from propagating the errors of the coefficients. Instead, we run the integration with the results for the coefficients a_i, Eq. (39), of four different fits. The spread of the results serves as rough estimate of the error. Let us first check the consistency with the results given in Table IV. Let us consider $(\lambda_1, \mu_1) = (3.8, -1.2)$ and $(\lambda_2, \mu_2) = (4.2, -1.1)$ as example, where $\overline{U}_C = 0.179\,833(39)$ and $0.139\,891(65)$ for $L = 64$, respectively. Running Eq. (31) with the coefficients obtained from four different fits, we arrive at the estimate of the scale factor $c_{1,2} = 4.70(12)$, which can be compared with $c_{1,2} = 1.33(1) \times 3.35(4) = 4.46(9)$ taken from Table IV. Next we computed the scale factor $c_{1,2}$ between $(\lambda_1, \mu_1) = (3.8, -1.2)$ and $(\lambda_2, \mu_2) = (4.5, -0.8)$, $(4.7, -0.6)$, and $(5.0, -0.3)$ by using Eq. (39) as examples. We get $c_{1,2} = 562.(26.0)$, $152\,000.0(17\,000.0)$, and $3.9(1.0) \times 10^{13}$, respectively. Hence, the correlation length in the high-temperature phase at the transition temperature should be $\xi_{high} = 1\,960\,000.0(90\,000.0)$, $5.5(6) \times 10^8$, and $1.3(3) \times 10^{17}$, respectively. Note that the estimates of the error are only rough ones. Still the order of magnitude of ξ_{high} should be correct. It is apparent that the range of parameters, where the first-order transition is very weak, is large.

V. EFFECTIVE EXPONENT OF THE CORRELATION LENGTH

In Ref. [8] the authors suggest that for a weak first-order transition, for a large range of reduced temperatures, the behavior of the correlation length is similar to that at a second-order phase transition, where however the exponent ν of the O(3)-invariant Heisenberg universality class is replaced by an effective one that depends weakly on the reduced temperature.
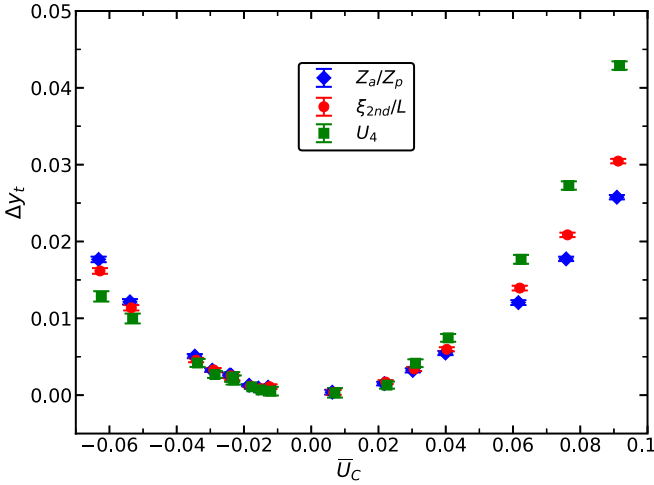
FIG. 6. We plot Δy_t, Eq. (42), obtained for a large set of (λ, μ) as a function of $\overline{U}_C$. Details are discussed in the text.

Here we analyze the finite-size scaling behavior of the slope of dimensionless quantities and the behavior of the infinite-volume correlation length in the high-temperature phase.

A. Finite-size scaling

We analyze the slopes S_i of dimensionless quantities $\tilde{R}_i = R_i - \sum_{j=2}^{m} c_{i,j} U_C^j$ at β_f, where $S_i = \partial \tilde{R}_i / \partial \beta$. The idea is that $\tilde{R}_i$ stays approximately constant with increasing L at the transition temperature, and that this hopefully also improves the behavior of the slope S_i. We redo the analysis of Sec. VII D of Ref. [6] with new data added. Note that in Ref. [6] we have used by mistake the wrong sign for the improvement term $\sum_{j=2}^{m} c_{i,j} \overline{U}_C^j$. Here we compare final results obtained by using different choices of $c_{i,j}$.

Since we are interested in the difference compared with the Heisenberg universality class, we analyze ratios

$$r_{S,i}[(\lambda, \mu), (\lambda_0, 0), L] = \frac{S_{\lambda,\mu,i}(L)}{S_{\lambda_0,\mu=0,i}(L)}, \qquad (41)$$

where i indicates which dimensionless quantity is taken and $\lambda_0 = 5.2$ or 5.0. Note that $\lambda^* = 5.12(5)$ for $\mu = 0$ (see Sec. IV A). We expect that subleading corrections approximately cancel. Therefore, we analyze the ratio with the simple *Ansatz*

$$r_{S,i}[(\lambda, \mu), (\lambda_0, 0), L] = a L^{\Delta y_t}. \qquad (42)$$

We performed fits for a number of values of (λ, μ) using a minimal lattice size $L_{\min} = 16$ or 24 that is taken into account. In Fig. 6 we plot Δy_t obtained by using $L_{\min} = 24$ and $\lambda_0 = 5.2$ as a function of $\overline{U}_C$. The values of $c_{i,j}$ are taken from Table I and $m = 4$. Here β_f is obtained from fixing $Z_a/Z_p - \sum_{j=2}^{m} c_{i,j} U_C^j = 0.19477$ using the values of $c_{i,j}$ given in Table I. As argument of Δy_t we take $[\overline{U}_C(L_{\max}) + \overline{U}_C(L_{\min})]/2$, where $L_{\max}$ and $L_{\min}$ are the largest and the smallest lattice sizes taken into account in the fit.

We have analyzed the estimates of Δy_t by using the *Ansätze*

$$\Delta y_t = b\overline{U}_C^2 + c\overline{U}_C^3 \qquad (43)$$

and

$$\Delta y_t = b\overline{U}_C^2 + c\overline{U}_C^3 + d\overline{U}_C^4 \qquad (44)$$

for the three different dimensionless quantities with different choices for $\sum_{j=2}^{m} c_{i,j} \overline{U}_C^j$.

For $c_{i,j} = 0$, already the estimate of b depends on the dimensionless quantity that is considered. For example, from a fit with $L_{\min} = 16$ and $\lambda_0 = 5.2$ we get $b = 3.94(3)$, $4.21(3)$, and $3.55(5)$ for Z_a/Z_p, $\xi_{2\text{nd}}/L$, and U_4, respectively. In all three cases we used the *Ansatz* (43) and data for $-0.06 \lesssim \overline{U}_C \lesssim 0.06$. We added successively higher orders of $\overline{U}_C$ to define $\tilde{R}_i$. We could not identify a clean convergence pattern for the coefficients of Eqs. (43) and (44).

For the choice of $c_{i,j}$ used for the data given in Fig. 6, we find that the results for b are more or less the same for the three different dimensionless quantities. We quote

$$b = 3.8(2) \qquad (45)$$

as our final result. For c, the results depend clearly on the dimensionless quantity that is considered. Certainly, deeper theoretical insight is needed to decide whether a unique effective exponent ν_{eff} can be obtained from finite-size scaling.

Note that at the cubic fixed point, for finite m and any choice of $c_{i,j}$, one should get in the limit $L \to \infty$ a unique value for Δy_t, not depending on the choice of the dimensionless quantity. Indeed, analyzing various choices $\sum_{j=2}^{m} c_{i,j} \overline{U}_C^j$, we get similar numerical estimates for Δy_t at the cubic fixed point for Z_a/Z_p, $\xi_{2\text{nd}}/L$, and U_4. In particular, we confirm the numerical results of Sec. VII D of Ref. [6]. In particular, plugging in the numerical estimate of $\overline{U}_C^*$ obtained in Sec. IV B above we get

$$y_{t,\text{cubic}} - y_{t,O(3)} = 3.8(2) \times [-0.0181(14)]^2 = 0.00124(12), \qquad (46)$$

where we have ignored $O(\overline{U}_C^{*3})$ contributions and have added up the errors due to b, Eq. (45), and $\overline{U}_C^*$.

B. Correlation length in the high-temperature phase

Here we have simulated the model for the two selected values $(\lambda, \mu) = (4.5, -0.8)$ and $(3.8, -1.2)$ in the high-temperature phase, where the correlation length can be determined very accurately by using the improved estimator of the correlation function that comes with the single-cluster algorithm [28]. For comparison we study $\lambda = 5.0$ and 5.2 at $\mu = 0$.

As estimate of the correlation length we take the effective correlation length

$$\xi_{\text{eff}}(t) = -\ln[G(t+1)/G(t)], \qquad (47)$$

where $G(t) = \langle \vec{S}(0) \cdot \vec{S}(t) \rangle$ and

$$\vec{S}(x_0) = \sum_{x_1, x_2} \vec{\phi}_{x_0, x_1, x_2}. \qquad (48)$$

Computing $G(t)$, we summed over all translations and all three directions on the lattice.

In the numerical analysis we improved Eq. (47) by taking into account periodic boundary conditions

$$G(\tau) = c\{\exp(-\tau/\xi_{\text{eff}}) + \exp[-(L-\tau)/\xi_{\text{eff}}]\}. \qquad (49)$$

Equation (49), for $\tau = t$ and $t + 1$, is solved for ξ_{eff} numerically. It turns out that $\xi_{\text{eff}}(t)$ is rapidly converging with increasing distance t. As our final estimate we take $\xi_{\text{eff}}(t)$ at $t = 2\xi_{\text{eff}}(t)$, self-consistently. We take a linear lattice size $L \approx 20\xi_{\text{eff}}$. We checked that for this lattice size finite-size effects are clearly negligible.

We performed simulations for a range of β such that $\xi \approx 2$ for the smallest value of β and $\xi \approx 10$ for the largest. We simulated at 26, 29, 34, and 36 different values of β for $(\lambda, \mu) = (3.8, -1.2)$, $(4.5, -0.8)$, $(5.0, 0)$, and $(5.2, 0)$, respectively. We performed at least 10^5 update cycles for each simulation. The update cycle consists of local Metropolis updates and single-cluster updates. We performed roughly as many single-cluster updates, such that, on average, the volume of the lattice is covered.

Assuming that the models are improved, we fitted our data with the simple *Ansatz*

$$\xi = at^{-\nu_{\text{eff}}} (1 + bt), \tag{50}$$

where we have included leading analytic corrections. Our definition of the reduced temperature is $t = \beta_t - \beta$. In a way, along with the range of β that is taken into account in the fit, this defines an effective value of the correlation length exponent ν. We took the estimate of β_t from the finite-size scaling analysis discussed above. The parameters of the fit are a, b, and ν_{eff}.

Fitting all our data for $(\lambda, \mu) = (5.2, 0)$ we get $\chi^2/\text{DOF} = 1.237$ corresponding to $p = 0.164$ and $\nu_{\text{eff}} = 0.710\,45(8)$, which is slightly too small compared with $\nu = 0.711\,64(10)$ [23] or $\nu = 0.711\,69(30)$ [7]. Discarding small values of β, the fit improves and the value of ν increases. For example, taking $\beta = 0.65$ with $\xi = 3.258\,46(24)$ as minimal value, we get $\chi^2/\text{DOF} = 1.005$ corresponding to $p = 0.455$ and $\nu_{\text{eff}} = 0.710\,93(22)$. The small deviation of ν_{eff} from the estimates of Refs. [7,23] can be attributed to corrections not taken into account in the *Ansatz* (50). Analyzing the data for $(\lambda, \mu) = (5.0, 0)$ we get $\chi^2/\text{DOF} = 0.999$ corresponding to $p = 0.467$ and $\nu_{\text{eff}} = 0.710\,24(8)$. Also in this case, χ^2/DOF decreases, when discarding small values of β and the value of ν_{eff} slightly increases. For example, for the minimal value $\beta = 0.65$ with $\xi = 3.274\,36(28)$ we get $\chi^2/\text{DOF} = 0.680$, $p = 0.870$, and $\nu_{\text{eff}} = 0.710\,95(24)$.

In summary, using the simple *Ansatz* (50) taking data for $\xi \approx 3.3$ up to $\xi \approx 10$ we obtain an estimate of ν that deviates from the most accurate values for the Heisenberg universality class, given in the literature, in the fourth digit.

Now let us turn to the data for $\mu < 0$. For $(\lambda, \mu) = (4.5, -0.8)$ we get $\chi^2/\text{DOF} = 1.550$, $p = 0.0365$ taking into account all data. We get $\nu_{\text{eff}} = 0.702\,35(9)$. The quality of the fit does not improve discarding data. We note that our numerical estimates of ξ are very accurate and less accurate data might result in an acceptable fit. The estimate of ν_{eff} is clearly smaller than those obtained for $\mu = 0$. The deviation is about 1%.

Finally, we analyzed our data for $(\lambda, \mu) = (3.8, -1.2)$. Fitting all data we get $\chi^2/\text{DOF} = 5.054$, $p = 0.000$, and $\nu_{\text{eff}} = 0.683\,82(8)$. Here, discarding data, keeping $\beta = 0.64$, $\xi = 3.612\,72(27)$ as smallest value of β we get $\chi^2/\text{DOF} = 1.309$, $p = 0.199$, and $\nu_{\text{eff}} = 0.681\,76(27)$, which is clearly smaller than the O(3)-invariant value. Fitting all data up to

$\beta = 0.648$, $\xi = 4.503\,59(34)$, we get $\chi^2/\text{DOF} = 0.692$, $p = 0.733$, and $\nu_{\text{eff}} = 0.685\,19(28)$. We notice that the value of ν_{eff} decreases, decreasing the reduced temperature t.

In order to compare the result obtained here with that obtained from finite-size scaling, we take $\overline{U}_C$ as defined in Sec. IV B for $L = 8$ at $(\lambda, \mu) = (4.5, -0.8)$ and $(3.8, -1.2)$, where $L = 8$ is chosen to have a rough match with the correlation lengths up to $\xi \approx 10$ that are considered here. We estimate $\overline{U}_C \approx 0.0678$ and 0.1177, respectively. Hence, we get $y_{t,\text{eff}} \approx 1.4052 + 3.8\overline{U}_C^2 \approx 1.4227$ and 1.4578, corresponding to $\nu_{\text{eff}} \approx 0.7029$ and 0.6859, respectively. These numbers are in reasonable agreement with the results obtained from the correlation length in the high-temperature phase.

VI. FIRST-ORDER PHASE TRANSITION

Here we discuss our simulations for values of (λ, μ), where the first-order transition is sufficiently strong such that it can be detected directly in the analysis of the data generated in the simulation. We performed extensive preliminary simulations to get an idea of the range of (λ, μ), where this is the case. A first indication of a first-order transition is the appearance of metastabilities in standard simulations. Furthermore, it is useful to study the histograms of various observables. At first-order transitions, double-peak structures appear. These double peaks become sharper and clearer separated as the linear lattice size increases. The separation of the peaks is accompanied by a rapid increase of the autocorrelation time with increasing lattice size, when using standard algorithms.

Below, we briefly discuss our implementation of the multicanonical method [29,30] that at least mitigates the problem of the increasing autocorrelation time. For more detailed discussions and alternatives to the multicanonical method see, for example, Refs. [31–35]. Then we discuss our numerical results for the transition temperatures, the interface tension, the latent heat, and the correlation length in the high-temperature phase at the transition. The theoretical basis for the finite-size scaling analysis of first-order phase transitions is provided by Refs. [17,36].

A. Multicanonical method

In order to perform simulations for lattices with $L \gg \xi_{\text{high}}$ at the transition temperature, we employed the multicanonical method [29,30]. In standard simulations, using a local algorithm, configurations can be changed only in small steps. Hence, going from the disordered to an ordered phase and vice versa, the Markov chain has to pass configurations, where both phases are present, separated by interfaces. These configurations are highly suppressed and their weight is decreasing exponentially with the area of the interfaces. Therefore, in the simulation these configurations are rarely visited and hence tunneling times between the phases become larger and larger as the lattice size increases.

The basic idea of the multicanonical method is to simulate a modified distribution such that configurations that contain two phases have an enhanced probability compared with the Boltzmann distribution. Configurations $\{\vec{\phi}\}$ are generated with

a probability distribution

$$P(\{\vec{\phi}\}) = \frac{1}{\sum_{\{\vec{\phi}\}} \exp(-H[\{\vec{\phi}\}])W(X[\{\vec{\phi}\}])}$$
$$\times \exp(-H[\{\vec{\phi}\}])W(X[\{\vec{\phi}\}]), \qquad (51)$$

where $W(X[\{\vec{\phi}\}])$ is a real positive number and $X[\{\vec{\phi}\}]$ is an estimator of an observable. In our simulations we took the energy, Eq. (9), for this purpose. Using the multicanonical method the problem of the increasing tunneling time can be drastically reduced but not completely eliminated. For a discussion see, for example, Ref. [37].

The expectation value of an estimator $A[\{\vec{\phi}\}]$ with respect to the Boltzmann distribution is given by

$$\langle A \rangle \approx \frac{\sum_i W^{-1}(X[\{\vec{\phi}\}_i])A[\{\vec{\phi}\}_i]}{\sum_i W^{-1}(X[\{\vec{\phi}\}_i])}, \qquad (52)$$

where we sum over the configurations that are generated after equilibration.

The function $W(X)$ should be constructed such that the histogram becomes essentially flat between the maxima of the Boltzmann distribution. We construct $W(X)$ as a piecewise constant function:

$$W(X) = \begin{cases} 1 & \text{for} \quad X < X_0, \\ w_i & \text{for} \quad X_0 + i\Delta \leqslant X < (i+1)\Delta, \\ 1 & \text{for} \quad X_1 < X, \end{cases} \qquad (53)$$

where $i \in \{0, 1, \ldots, M-1\}$ and $\Delta = (X_1 - X_0)/M$. X_0 and X_1 roughly give the position of the peaks in the histogram. In our simulations $10 \leqslant M \leqslant 600$. The weights w_i are computed from the histogram. They can be iteratively improved by using more and more accurate data for the histogram. For lattice sizes that are not too large, one gets a few tunnelings between the phases by simulating with the Boltzmann distribution and one can use these simulations as starting point for the iterative determination of $W(X)$.

In case one has a reasonable *Ansatz* for the histogram of X as a function of the linear lattice size L, one might increment L in small steps. A first guess for $W(X)$ might be obtained by extrapolating the results obtained for the lattice sizes simulated before.

Here we did not succeed with such a strategy. Instead, we proceed without using the knowledge obtained from the simulation of smaller lattice sizes: we started with two simulations taking $W(X) = 1$ for all X. These simulations are started with configurations that are in the domain of the disordered and the ordered phase, respectively. For the disordered phase we take

$$\phi_{x,i} = \text{rand} - 0.5 \qquad (54)$$

for all sites x and components i, where rand is a uniformly distributed random number in the interval [0,1]. In the case of the ordered phase we take

$$\phi_{x,0} = \Phi_0 + \text{rand} - 0.5 \qquad (55)$$

and

$$\phi_{x,i} = \text{rand} - 0.5 \qquad (56)$$

for $i > 0$, where Φ_0 is a rough approximation of the expectation value of the field in the ordered phase.

For sufficiently large lattice sizes L, the probability that the simulation switches the phase during the simulation is virtually vanishing. We compute the histograms of X for these two simulations. We chose X_0 as the position of the maximum of the histogram of the disordered simulation and X_1 as the position of the maximum of the histogram of the ordered simulation. Typically, we get reasonable statistics only up to $X_0 + \epsilon_0$ and down to $X_1 - \epsilon_1$. In the middle, there is a gap without any configuration generated. We compute $W(X)$ up to $X_0 + \epsilon_0$ and and down to $X_1 - \epsilon_1$ straightforwardly from the histogram. The gap between $X_0 + \epsilon_0$ and $X_1 - \epsilon_1$ is filled by linear interpolation. We also experimented with guessing somewhat larger values of $W(X)$ in the gap to speed up the convergence. We iterated this step until the gap has closed. Then we proceeded as above.

We performed the simulations using a hybrid of local Metropolis, local over-relaxation, and wall-cluster [25] updates. The weight W is integrated in the accept or reject step of the local algorithms in the straightforward way. In the case of the wall-cluster algorithm, the cluster is constructed following the same rules as for the plain Boltzmann distribution. The update of the wall cluster is viewed as a proposal of a Metropolis step, where the accept or reject step takes into account the change of W caused by the wall-cluster update:

$$P_{\text{acc}} = \min[1, W(X[\{\vec{\phi}\}'])/W(X[\{\vec{\phi}\}])], \qquad (57)$$

where $\{\vec{\phi}\}'$ is the configuration that results from the wall-cluster update of $\{\vec{\phi}\}$.

B. Simulations at the first-order transition

Based on our preliminary studies we focused on simulations for the five pairs of parameters: $(\lambda, \mu) = (1.24, -2.3)$, $(1.675, -1.95)$, $(2.0, -1.85)$, $(3, -2.5)$, and $(2.333, -1.764)$. These values were selected such that the correlation length in the high-temperature phase at the transition temperature is about $\xi_{\text{high}} \approx 2, 6, 12, 12$, and 24, respectively. The smaller ξ_{high}, the stronger is the first-order transition.

First, for all pairs of parameters, we performed simulations with the program used in Ref. [6], generating configurations following the Boltzmann distribution. It can be used as long as the tunneling times between the phases are not too large. We performed such simulations using the linear lattice size $L = 8$ for $(\lambda, \mu) = (1.24, -2.3)$, $L = 12, 16$, and 24 for $(\lambda, \mu) = (1.675, -1.95)$, $L = 12, 16, 20, 24, 32, 40$, and 48 for $(\lambda, \mu) = (2, -1.85)$, $L = 12, 16, 20, 24$, and 32 for $(3, -2.5)$, and $L = 12, 16, 20, 24, 32, 40, 48$, and 64 for $(\lambda, \mu) = (2.333, -1.764)$. We extracted a preliminary estimate of the transition temperature by requiring that $Z_a/Z_p = \frac{1}{7}$. Larger lattice sizes were simulated by using the multicanonical method as discussed above. We started the detailed study of the transition for $(\lambda, \mu) = (1.24, -2.3)$, where we simulated the linear lattice sizes $L = 8, 12, 16, 24, 28, 32$, and 40.

In our program no parallelization is implemented. We employed trivial parallelization at a moderate level: In the case of $L = 40$ we performed five independent simulations with

TABLE V. Estimates of the transition temperature β_t and the interface free energy F_I, up to a constant, for a range of linear lattice sizes L at $(\lambda, \mu) = (1.24, -2.3)$. For a discussion see the text.

| L	β_t	$2F_I + C$
8	0.329460(25)	9.12(7)
12	0.329409(9)	16.30(4)
16	0.329405(6)	28.01(5)
24	0.3294116(20)	65.07(6)
28	0.3294096(19)	89.01(8)
32	0.3294099(9)	115.76(6)
40	0.3294108(5)	178.90(10)

FIG. 7. We give the histograms of the energy density at $(\lambda, \mu) = (1.24, -2.3)$ for the linear lattice sizes $L = 12$, 16, 24, 28, 32, and 40. The data are reweighted to the Boltzmann distribution for $\beta = 0.3294108$, which is our estimate of the inverse of the transition temperature.

ordered and five independent simulations with disordered start configurations in parallel. In a series of preliminary runs, as discussed above, we determine the weight function $W(X)$ for the multicanonical simulation.

The results given below are based on simulations using our final estimate of the weight function. Even when using the multicanonical simulation, autocorrelation times increase rapidly with increasing lattice size. In particular, in the case of larger lattice sizes one has to find a reasonable compromise, when discarding configurations for equilibration. We took $t_{\mathrm{dis}} \approx 10\tau_{\mathrm{ene}}$, where τ_{ene} is the integrated autocorrelation time of the energy. We inspected the history of our simulations by plotting the expectation values of the energy or the magnetic susceptibility versus the iteration number of the Markov chain. We find that with this choice of t_{dis}, a few tunnelings from disorder to order and vice versa are discarded. Errors are computed by jackknife binning with $N_{\mathrm{bin}} = 20$. The simulations were performed using a value of β slightly smaller than the preliminary estimate of β_t available when starting the simulation, giving more weight to the disordered phase.

For $L = 40$, we performed for each measurement 30 sweeps with a local update algorithm and 18 wall-cluster updates. With our final version of $W(X)$, we performed 5.5×10^7 measurements after equilibration. These simulations took about 120 days on a single core of an AMD EPYC™ 7351P CPU. The integrated autocorrelation time of the energy is about $\tau_{\mathrm{ene}} \approx 80\,000$ in units of measurements.

First we computed the inverse β_t of the transition temperature. To this end, we determined the location $E_{\min}$ of the minimum of the histogram of the energy density, reweighted to the Boltzmann distribution for a preliminary estimate of β_t. Then the estimate of β_t is computed by requiring that the total weight of configurations with $E \geqslant E_{\min}$ is $2N = 6$ times as large as that for $E < E_{\min}$. Since the probability density in the neighborhood of $E_{\min}$ is very small, the estimate of β_t is not very sensitive to the exact choice of $E_{\min}$. Preliminary analysis shows that replacing the energy by, for example, the square of the magnetization leads to virtually identical results. Our estimates of β_t are summarized in Table V. One expects that β_t is converging exponentially fast with increasing lattice size [17,36]. In fact, all estimates obtained for $L \geqslant 12$ are consistent among each other. As final result we take $\beta_t = 0.3\,294\,108(5)$, obtained for our largest linear lattice size $L = 40$. For $L = 8$, simulating the Boltzmann distribution and
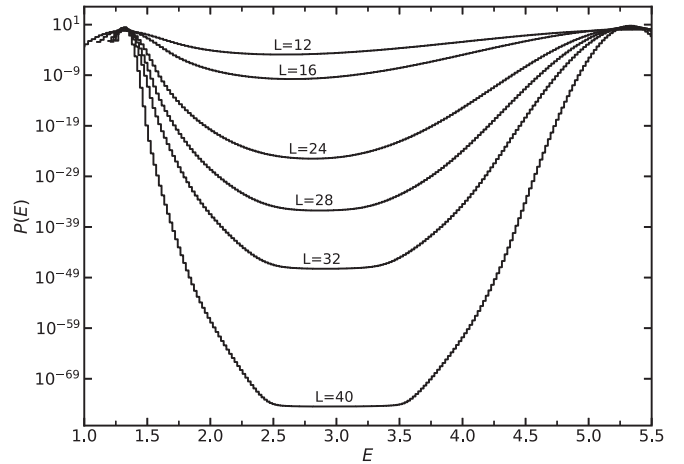
requiring that $Z_a/Z_p = \frac{1}{7}$ we get $\beta_t = 0.329\,405(9)$, which is compatible with our final result.

In Fig. 7 we plot the histograms for the energy density for the Boltzmann distribution at $(\lambda, \mu) = (1.24, -2.3)$, $\beta = 0.3\,294\,108$, and the lattice sizes we have simulated. Histograms at the first-order transition can be understood starting from an effective description of the configuration space. There are regions on the lattice that can be assigned to one of the phases. At the transition, all phases have the same free-energy density. These regions are separated by interfaces, which are characterized by their interface tension σ. The weight of these sets of configurations is given by the free energy of the interfaces.

An observable, for example, the energy density, takes a certain value for each of the phases. There is a characteristic variance of the observable for each of the phases. The peaks in the histogram are associated with configurations, where only one phase is present. To understand the histogram between the peaks we have to consider configurations, where two phases, the disordered phase and one of the ordered phases, are present. One has to consider configurations, which are predominantly associated with one of the phases, and there is a droplet of the other phase. Furthermore, on a L^3 lattice with periodic boundary conditions, for large L, the minimum in the histogram is related with configurations, where the phases are separated by two flat interfaces with the area L^2. The reduced free energy of a single interface is

$$F_I = \sigma L^2 + c, \tag{58}$$

where the constant c takes into account fluctuations of the interface. Since F_I does not depend on the distance between the interfaces, the histogram becomes flat at the minimum. Taking into account the translational invariance we get, up to a constant prefactor,

$$z_{2I}(L) = \exp[2\ln L - 2F_I(L)] \tag{59}$$

TABLE VI. Final estimates for the first-order phase transition. In the first column we give the value of the parameters (λ, μ), in the second column we give the inverse β_t of the transition temperature, in the third the interface tension for interfaces between the disordered and one of the ordered phases. In the fourth column we give the latent heat Q and, finally, in the fifth column the correlation length in the high-temperature phase. For a discussion see the text.

(λ, μ)	β_t	σ	Q	ξ_{high}
$(2.333, -1.764)$	0.60891779(23)	0.00046(5)	0.04218(15)	24.70(2)
$(3, -2.5)$	0.58194181(50)		0.1182(1)	12.33(2)
$(2, -1.85)$	0.57905753(56)	0.0019(1)	0.11681(7)	12.135(6)
$(1.675, -1.95)$	0.5306093(64)	0.0074(4)	0.3054(5)	6.003(2)
$(1.24, -2.3)$	0.3294108(5)	0.055(1)	1.2012(10)	1.9833(10)

as weight for the collection of configurations, where two phases are separated by two flat interfaces. We determine z_{2I} up to a constant prefactor by the value of the histogram at its minimum. Our numerical results for $2F_I(L) + C = -\ln[z_{2I}(L)] + 2 \ln L$ are summarized in Table V.

In order to determine the interface tension, we take two lattice sizes L_1 and L_2:

$$\sigma = \frac{F_I(L_2) - F_I(L_1)}{L_2^2 - L_1^2}. \tag{60}$$

We arrive at $\sigma = 0.0449(5)$, $0.0523(3)$, $0.0579(1)$, $0.0566(1)$, and $0.0548(1)$ for $(L_1, L_2) = (8, 12)$, $(12, 16)$, $(16, 24)$, $(24, 32)$, and $(32, 40)$. The histograms plotted in Fig. 7 show only a clean plateau value between the peaks for $L = 40$ and to a reasonable approximation for $L = 32$. Therefore, we take our estimate obtained for $(L_1, L_2) = (32, 40)$ as final result.

We performed simulations by using the multicanonical method for weaker first-order phase transitions in a similar fashion as for $(\lambda, \mu) = (1.24, -2.3)$. The largest lattice sizes that we have reached are $L_{\max} = 64, 96, 64$, and 128 for $(\lambda, \mu) = (1.675, -1.95)$, $(2.0, -1.85)$, $(3.0, -2.5)$, and $(2.333, -1.764)$, respectively. Our final results for β_t and σ are given in Table VI. Here our largest L/ξ_{high} are smaller than for $(\lambda, \mu) = (1.24, -2.3)$. Therefore, systematic errors computing σ by using Eq. (60) are present. We corrected for that by taking into account the dependence of the estimate of σ seen for $(\lambda, \mu) = (1.24, -2.3)$ as a function of L/ξ_{high}.

1. Correlation length

In order to compute the correlation length in the disordered phase at the transition temperature, we simulated the model by using the same program as above in Sec. V. The simulations are started with $\phi_{x,i} = \text{rand} - 0.5$ for all sites x and components i. The linear lattice size L is chosen such that the tunneling time to an ordered phase is very large compared with the length of the simulation. To this end, we use $L \approx 20\xi_{\text{high}}$, self-consistently. The correlation length is determined as discussed above in Sec. V. Our final results are summarized in Table VI. The errors quoted take the uncertainty of the inverse transition temperature β_t into account.

Computing the correlation length for the ordered phases turns out to be considerably more difficult. Here, the connected part of the correlation function has to be computed. The improved estimator proposed for models with Z_2 symmetry [38] can not be applied. Furthermore, the effective correlation length converges more slowly than in the disordered phase.

Therefore, we computed the correlation length for the ordered phases only for $(\lambda, \mu) = (1.24, -2.3)$. We get the rough estimate $\xi_{\text{low}} = 1.6(1)$.

2. Latent heat

We define the latent heat as

$$Q = \frac{1}{L^3}(\langle \mathcal{H} \rangle_{\text{disorder}} - \langle \mathcal{H} \rangle_{\text{order}}) \tag{61}$$

taken at the transition temperature β_t. For the disordered phase, the measurements are taken from a subset of the simulations done for the correlation length discussed above. For the ordered phases, we performed simulations with the same lattice sizes as for the ordered phase. The simulations are started with a configuration generated by using Eqs. (55) and (56). Our results are given in Table VI.

3. Scaling of the interface tension and the latent heat

As the first-order phase transition becomes weaker, the interface tension and the latent heat decrease. The combination $\sigma \xi_{\text{high}}^2$ should have a finite limit as the O(3)-invariant fixed point is approached. In fact, we find $\sigma \xi_{\text{high}}^2 = 0.216(4)$, $0.267(15)$, $0.280(15)$, and $0.28(3)$ for $(\lambda, \mu) = (1.24, -2.3)$, $(1.675, -1.95)$, $(2.0, -1.85)$, and $(2.333, -1.764)$, respectively. As our estimate for the scaling limit, we quote $\sigma \xi_{\text{high}}^2 = 0.28(3)$.

In the case of the latent heat we expect from dimensional analysis that

$$Q \xi_{\text{high}}^{d - y_t} = Q \xi_{\text{high}}^{\Delta_\epsilon}, \tag{62}$$

where y_t is the thermal RG exponent of the Heisenberg universality class, approaches a finite limit as the Heisenberg fixed point is approached.

Taking $y_t = 1.4052(2)$ [23], we get $Q \xi_{\text{high}}^{\Delta_\epsilon} = 3.580(4)$, $5.324(9)$, $6.256(6)$, $6.494(18)$, and $7.017(27)$ for $(\lambda, \mu) = (1.24, -2.3)$, $(1.675, -1.95)$, $(2.0, -1.85)$, $(3.0, -2.5)$ and $(2.333, -1.764)$, respectively. Here the convergence is not as convincing as for the interface tension. We abstain from quoting a result for the limit $\xi_{\text{high}} \to \infty$.

VII. SUMMARY AND CONCLUSION

We have studied the three-component ϕ^4 model on the simple cubic lattice with a cubic perturbation. Field theory predicts that the RG flow rapidly collapses onto a single line in coupling space. On this line the RG flow remains

slow in an extended range and not just in the vicinity of the fixed points. See, for example, Ref. [8]. Here we corroborate this picture by using Monte Carlo simulations in connection with a finite-size scaling analysis. To this end, compared with Ref. [6], we have extended the study towards stronger breaking of the O(3) invariance. In a preliminary step, we identify the line of slow flow in the parameters (λ, μ) of the reduced Hamiltonian (3). Here we obtain a more accurate characterization than in Ref. [6]. Next we study the slow RG flow in the scaling limit. This limit is reached faster for (λ, μ) on the line of slow flow than for generic choices. In particular at the fixed points, corrections proportional to $L^{-\omega}$ with $\omega \approx 0.8$ should be essentially eliminated. Remaining corrections are proportional to $L^{-\epsilon_j}$ with $\epsilon_j \gtrsim 2$. Note that the slow RG flow is not studied in terms of the parameters of the reduced Hamiltonian but by using the dimensionless quantity U_C [Eq. (14)] at criticality that quantifies the violation of the O(3) symmetry. Numerically we determine the coefficients of the β function [Eqs. (22), (31), and (39)] for U_C. The analysis of the β function provides us with an accurate estimate of the difference $Y_4 - \omega_2 = 0.00081(7)$, where Y_4 is the RG exponent of the cubic perturbation at the O(3)-symmetric fixed point and ω_2 the correction exponent at the cubic fixed point. Note that for $a_{i \geqslant 2} = 0$ [Eq. (39)], $Y_4 = \omega_2$. For example, in Refs. [8,39] this approximation of the β function is considered. Here, analyzing the β function we get $Y_4 = 0.0141(10)$. In Ref. [6], repeating the FSS analysis at the O(3)-symmetric fixed of Ref. [5] with higher statistics, we arrived at $Y_4 = 0.0143(9)$, which is fully consistent. These two approaches are technically very different, giving us further confidence in the reliability of the estimates.

In Sec. V, motivated by Ref. [8], we determine an effective exponent ν_{eff} of the correlation length. First we perform a FSS analysis, which provides estimates of ν_{eff} as a function of U_C. Then we analyze the behavior of the correlation length in the high-temperature phase for two values of (λ, μ) with $\mu < 0$. The results obtained by these two different approaches are in reasonable agreement.

In the final part of the study we focus on the first-order phase transition. For a strong breaking of the O(3) invariance we clearly confirm the first-order nature of the transition. Histograms of various observables show a clear double-peak structure. The separation of the two peaks becomes stronger with increasing lattice size. We obtain accurate estimates of the latent heat, the correlation length in the disordered phase at the transition, and the interface tension of interfaces between the disordered and one of the ordered phases. We analyze how these quantities scale with the RG flow. This allows us to predict the strength of the transition for parameter values, where the transition is weak and can therefore not be identified as first-order directly in the simulations.

The RG flow numerically studied here is universal. Still, applied directly to experiments, only qualitative and semi-quantitative conclusion can be drawn. However, simulating more realistic models of experimental systems, one could determine the same dimensionless quantities as discussed here. In particular, computing U_C would connect quantitatively with the results obtained here.

APPENDIX A: QUALITY OF FITS AND ESTIMATING ERRORS

We perform a standard analysis of our data by using least-square fits as discussed, for example, in Ref. [40]. Let us assume we have N uncorrelated data points $y_i = y(x_i)$ with a statistical error σ_i with a Gaussian distribution. These are fitted by using the *Ansatz*, or model in the language of statistics, $f(x; p_1, \ldots, p_M)$, where p_j are the parameters of the *Ansatz*. One defines

$$\chi^2 = \sum_i \frac{[y_i - f(x_i; p_1, \ldots, p_M)]^2}{\sigma_i^2}. \quad (A1)$$

In the case of correlations, given by the covariance matrix C, this generalizes to

$$\chi^2 = \sum_{ij} [y_i - f(x_i, p_1, \ldots, p_M)](C^{-1})_{ij}$$
$$\times [y_j - f(x_j, p_1, \ldots, p_M)]. \quad (A2)$$

For given y_i and σ_i or C, the parameters p_j are obtained by minimizing χ^2. To this end, we employ the function curve_fit() contained in the SCIPY library [41]. The function curve_fit() acts as a wrapper to functions contained in the MINPACK library [42]. In selected cases, we checked the outcome of the fit by varying the initial values of the parameters. Furthermore, we performed fits both by using the Levenberg-Marquardt algorithm and the trust region reflective algorithm. In Sec. IV B, we compute numerically $\overline{U}_C^*$, ω_2, and $Y_4 - \omega_2$, based on the results for the parameters $a_0, a_1, \ldots, a_n$ of the fit, Eq. (39). In order to obtain the statistical error of these quantities, we compute the partial derivatives of these quantities with respect to the statistically independent data y_i, which are $\overline{U}_C$ for different (λ, μ) and L in the present case. To this end, we repeat the fit N times, where N is the number of data points. For each of these fits, one of the y_i is shifted by a small amount: $\tilde{y}_i = y_i + \epsilon$ if $i = j$ and $\tilde{y}_i = y_i$ else. Then $\partial q / \partial y_j \approx (\tilde{q}_j - q) / \epsilon$. Here q is the estimate of one of the derived quantities obtained for the original data, while $\tilde{q}_j$ is the result obtained for y_j shifted. Then the statistical error σ_q is given by

$$\sigma_q^2 = \sum_{j=1}^{N} \left[\frac{\partial q}{\partial y_j} \right]^2 \sigma_j^2. \quad (A3)$$

To check the correctness of the implementation, we also computed the statistical error of the parameters $a_0, a_1, \ldots, a_n$ this way, giving results consistent with those provided by the function curve_fit(). Alternatively, one could compute the partial derivatives of q with respect to the parameters $a_0, a_1, \ldots, a_n$ and then use the covariance matrix provided by curve_fit() to compute the statistical error of q.

In order to assess χ^2 we compute

$$p(n_{\text{DOF}}, \chi^2) = \frac{1}{\Gamma(n_{\text{DOF}}/2)} \int_{\chi^2/2}^{\infty} t^{n_{\text{DOF}}/2 - 1} \exp(-t) dt, \quad (A4)$$

where Γ is the Euler gamma function and $n_{\text{DOF}} = N - M$ the number of degrees of freedom. In the Numerical Recipes, Sect. 15 [43] or Ref. [40], this quantity is denoted as goodness of the fit. The meaning of this quantity is derived for linear *Ansätze* (see, for example, Appendix C of Ref. [40]). For small values of the errors, this should also apply to nonlinear *Ansätze*. In the broader context of statistics, the goodness of the fit is the p value for the null hypothesis that the *Ansatz* is correct, without any correction. Assuming that the null hypothesis is correct, the p value gives the probability that the data drawn give the value of χ^2 we obtain or larger. For small p values one rejects the null hypothesis. Typically, in the literature, a fit with $p \geqslant 0.05$ or 0.1 is considered to be not excluded. In the text we frequently write sloppily that the fit is acceptable.

As usual, we perform fits by using a number of different *Ansätze*, with a varying degree of approximation compared with the exact form, which is typically only known in certain limits. In a first step, these fits are evaluated based on their $\chi^2/$DOF and the goodness of the fit obtained from this. Frequently in the literature a best fit is selected among those that have an acceptable $\chi^2/$DOF and p value. The parameter values obtained from this best fit are presented as the final results, including the statistical error estimates obtained by the fit. Implicitly it is assumed that systematic errors, caused by the imperfection of the *Ansatz*, are at most of the same size as the statistical errors. However, experience shows that this, depending on the type of the approximation, is often not the case and the systematic errors are way larger. One can easily convince oneself of this fact by generating numbers with a known function, put some Gaussian noise on it, and then fit these numbers by an *Ansatz* that is an approximation of the function we started with.

In order to get a better grasp on systematic errors, our final results are based on a number n_{fit} of fits using different *Ansätze*, with a varying degree of approximation compared with the exact form. Let us assume that we get a_α with the statistical error σ_α for the parameter a of the fits $\alpha = 1, 2,...,n_{\text{fit}}$. Then we quote $(a_{\max} + a_{\min})/2$ as our final result, with the error $(a_{\max} - a_{\min})/2$, where $a_{\max} = \max_\alpha [a_\alpha + \sigma_\alpha]$ and $a_{\min} = \min_\alpha [a_\alpha - \sigma_\alpha]$. In the text we write that the final result covers the estimates obtained by the fits $\alpha = 1, 2,...,n_{\text{fit}}$, which are taken into account. Obviously, the final error that is quoted is larger or equal than the statistical error of each of the fits. The reliability of the error estimate depends mainly on the choice of the fits that are taken into account. If they all suffer from the major source of systematic error in the same way, this error is not reflected in our error estimate.

Finally, let us note that we generated the plots by using the MATPLOTLIB library [44].

APPENDIX B: ANALYTIC RESULTS FOR THE β FUNCTION

We discuss the β function truncated at third order:

$$\tilde{u}(x) = a_0 x + a_1 x^2 + a_2 x^3, \tag{B1}$$

where for the ease of the notation the coupling is denoted by x. The indices of a_i are adjusted to the powers in $u(x) = \tilde{u}(x)/x$. The RG fixed points are given by the zeros of $\tilde{u}(x)$. The first zero $x = 0$ we find trivially. Factoring out this zero, we get

$$u(x) = a_0 + a_1 x + a_2 x^2. \tag{B2}$$

Let us first discuss the additional simplification $a_2 = 0$: the zero of $u(x)$ is given by $x = -a_0/a_1$. The RG exponents are given by the derivatives of the β function at the zeros:

$$\tilde{u}'(x) = a_0 + 2a_1 x + 3a_2 x^2. \tag{B3}$$

The RG exponent at $x = 0$ is $Y_4 = a_0$, irrespectively from the order of the truncation. For $a_i = 0$ for $i \geqslant 2$, we get for the zero $x = -a_0/a_1$ the RG exponent

$$\tilde{u}'(-a_0/a_1) = -\omega_2 = a_0 + 2a_1(-a_0/a_1) = -a_0. \tag{B4}$$

Hence, for the truncation $a_i = 0$ for $i \geqslant 2$ we have $Y_4 = \omega_2$.

The solutions of Eq. (B2) for $a_2 \neq 0$ are

$$x_{1/2} = \frac{-a_1 \pm \sqrt{a_1^2 - 4a_0 a_2}}{2a_2}. \tag{B5}$$

In order to get the solution close to $x = -a_0/a_1$ for small a_2, we have to select the $+$ from $\pm$. Expanding the square root for small a_2, we get

$$
\begin{aligned}
x_1 &= \frac{a_1\left(-1 + \sqrt{1 - 4a_0 a_2/a_1^2}\right)}{2a_2} \\
&= -a_0/a_1 - a_2 a_0^2/a_1^3 - \cdots .
\end{aligned} \tag{B6}
$$

The derivative of $\tilde{u}(x)$ at this zero is

$$
\begin{aligned}
\tilde{u}'(x_1) &= a_0 + 2a_1\left(-a_0/a_1 - a_2 a_0^2/a_1^3 - \cdots\right) \\
&\quad + 3a_2(a_0/a_1 + \cdots)^2 \\
&= -a_0 - 2a_2 a_0^2/a_1^2 + 3a_2(a_0/a_1)^2 + \cdots \\
&= -a_0 + a_2(a_0/a_1)^2 + \cdots .
\end{aligned} \tag{B7}
$$

Hence,

$$Y_0 - \omega_2 = a_2(a_0/a_1)^2 + \cdots . \tag{B8}$$

For the fits 1, 2, 3, and 4 of Sec. IV B, Table II, we get $a_2(a_0/a_1)^2 = 0.00063(4), 0.00063(2), 0.00066(1)$, and $0.00066(1)$, respectively. Hence, numerically $a_2(a_0/a_1)^2$ contributes more than $\frac{3}{4}$ of the value to $Y_0 - \omega_2$.

[1] A. Pelissetto and E. Vicari, Critical phenomena and renormalization-group theory, Phys. Rep. **368**, 549 (2002).

[2] J. Rong, Scalar CFTs from structural phase transitions, arXiv:2303.12028.

[3] L. Ts. Adzhemyan, E. V. Ivanova, M. V. Kompaniets, A. Kudlis, and A. I. Sokolov, Six-loop ϵ-expansion study of three-dimensional n-vector model with cubic anisotropy, Nucl. Phys. B **940**, 332 (2019).

[4] A. Bednyakov, J. Henriksson, and S. R. Kousvos, Anomalous dimensions in hypercubic theories, J. High Energy Phys. 11 (2023) 051.

[5] M. Hasenbusch and E. Vicari, Anisotropic perturbations in three-dimensional O(N)-symmetric vector models, Phys. Rev. B **84**, 125136 (2011).

[6] M. Hasenbusch, Cubic fixed point in three dimensions: Monte Carlo simulations of the model on the simple cubic lattice, Phys. Rev. B **107**, 024409 (2023).

[7] S. M. Chester, W. Landry, J. Liu, D. Poland, D. Simmons-Duffin, N. Su, and A. Vichi, Bootstrapping Heisenberg magnets and their cubic instability, Phys. Rev. D **104**, 105013 (2021).

[8] A. Aharony, O. Entin-Wohlman, and A. Kudlis, Different critical behaviors in cubic to trigonal and tetragonal perovskites, Phys. Rev. B **105**, 104101 (2022).

[9] A. Aharony, O. Entin-Wohlman, and A. Kudlis, Bi- and Tetra-critical phase diagrams in three dimensions, Low Temp. Phys. **48**, 483 (2022) [Fiz. Niz. Temp. (Kharkov) **48**, 542 (2022)].

[10] A. Aharony and O. Entin-Wohlman, Puzzle of bicriticality in the XXZ antiferromagnet, Phys. Rev. B **106**, 094424 (2022).

[11] A. Kudlis, A. Aharony, and O. Entin-Wohlman, Effective exponents near bicritical points, arXiv:2304.08265.

[12] M. Campostrini, M. Hasenbusch, A. Pelissetto, P. Rossi, and E. Vicari, Critical exponents and equation of state of the three-dimensional Heisenberg universality class, Phys. Rev. B **65**, 144520 (2002).

[13] F. J. Wegner, Critical exponents in isotropic spin systems, Phys. Rev. B **6**, 1891 (1972).

[14] M. Hasenbusch, A Monte Carlo study of leading order scaling corrections of ϕ^4 theory on a three dimensional lattice, J. Phys. A: Math. Gen. **32**, 4851 (1999).

[15] M. Campostrini, M. Hasenbusch, A. Pelissetto, P. Rossi, and E. Vicari, Critical behavior of the three-dimensional XY universality class, Phys. Rev. B **63**, 214503 (2001).

[16] M. Hasenbusch, Restoring isotropy in a three-dimensional lattice model: The Ising universality class, Phys. Rev. B **104**, 014426 (2021).

[17] C. Borgs and R. Kotecký, A rigorous theory of finite-size scaling at first-order phase transitions, J. Stat. Phys. **61**, 79 (1990).

[18] M. N. Barber, in *Finite-size Scaling in Phase Transitions and Critical Phenomena*, edited by C. Domb and J. L. Lebowitz (Academic, New York, 1983), Vol. 8.

[19] M. Lüscher, P. Weisz, and U. Wolff, A Numerical method to compute the running coupling in asymptotically free theories, Nucl. Phys. B **359**, 221 (1991).

[20] S. Caracciolo, R. G. Edwards, A. Pelissetto, and A. D. Sokal, Asymptotic scaling in the two-dimensional O(3) σ model at correlation length 10^5, Phys. Rev. Lett. **75**, 1891 (1995).

[21] J. Sak, Critical behavior of compressible magnets, Phys. Rev. B **10**, 3957 (1974).

[22] J. M. Carmona, A. Pelissetto, and E. Vicari, The N-component Ginzburg-Landau Hamiltonian with cubic anisotropy: A Six loop study, Phys. Rev. B **61**, 15136 (2000).

[23] M. Hasenbusch, Monte Carlo study of a generalized icosahedral model on the simple cubic lattice, Phys. Rev. B **102**, 024406 (2020).

[24] See Supplemental Material at http://link.aps.org/supplemental/10.1103/PhysRevB.109.054420 for estimates of the inverse transition temperature for a large set of parameter pairs (λ, μ).

[25] M. Hasenbusch, K. Pinn, and S. Vinti, Critical exponents of the 3D Ising universality class from finite size scaling with standard and improved actions, Phys. Rev. B **59**, 11471 (1999).

[26] F. Parisen Toldin, Finite-size scaling at fixed renormalization-group invariant, Phys. Rev. E **105**, 034137 (2022).

[27] F. Kos, D. Poland, D. Simmons-Duffin, and A. Vichi, Precision Islands in the Ising and $O(N)$ models, J. High Energy Phys. 08 (2016) 036.

[28] U. Wolff, Collective Monte Carlo updating for spin systems, Phys. Rev. Lett. **62**, 361 (1989).

[29] B. A. Berg and T. Neuhaus, Multicanonical algorithms for first order phase transitions, Phys. Lett. B **267**, 249 (1991).

[30] B. A. Berg and T. Neuhaus, Multicanonical ensemble: A new approach to simulate first-order phase transitions, Phys. Rev. Lett. **68**, 9 (1992).

[31] F. Wang and D. P. Landau, Efficient, multiple-range random walk algorithm to calculate the density of states, Phys. Rev. Lett. **86**, 2050 (2001).

[32] F. Wang and D. P. Landau, Determining the density of states for classical statistical models: A random walk algorithm to produce a flat histogram, Phys. Rev. E **64**, 056101 (2001).

[33] D. J. Earl and M. W. Deem, Parallel tempering: Theory, applications, and new perspectives, Phys. Chem. Chem. Phys. **7**, 3910 (2005).

[34] W. Janke, Multicanonical Monte Carlo simulations, Phys. A (Amsterdam) **254**, 164 (1998).

[35] W. Janke, Histograms and all that, in *Computer Simulations of Surfaces and Interfaces*, NATO Science Series, Vol. 114, edited by B. Dünweg, D. P. Landau, and A. I. Milchev (Springer, Dordrecht (2003).

[36] C. Borgs and W. Janke, New method to determine first-order transition points from finite-size data, Phys. Rev. Lett. **68**, 1738 (1992).

[37] B. Bauer, E. Gull, S. Trebst, M. Troyer and D. A. Huse, Optimized broad-histogram simulations for strong first- order phase transitions: droplet transitions in the large-Q Potts model, J. Stat. Mech. (2010) P01020.

[38] M. Hasenbusch, Variance-reduced estimator of the connected two-point function in the presence of a broken Z_2-symmetry, Phys. Rev. E **93**, 032140 (2016).

[39] J. Rong and N. Su, From $O(3)$ to Cubic CFT: Conformal perturbation and the large charge sector, arXiv:2311.00933.

[40] P. Young, *Everything You Wanted to Know About Data Analysis and Fitting but Were Afraid to Ask*, Springer Briefs in Physics (Springer, Berlin, 2015); https://doi.org/10.1007/978-3-319-19051-8.

[41] P. Virtanen, R. Gommers, T. E. Oliphant, M. Haberland, T. Reddy, D. Cournapeau, E. Burovski, P. Peterson, W. Weckesser, J. Bright *et al.*, SciPy 1.0: fundamental algorithms for scientific computing in Python, Nat. Methods **17**, 261 (2020).

[42] J. J. Moré, B. S. Garbow, and K. E. Hillstrom, User Guide for MINPACK-1, Argonne National Laboratory Report ANL-

80-74, 1980 (unpublished); J. J. Moré, D. C. Sorensen, K. E. Hillstrom, and B. S. Garbow, The MINPACK Project, in *Sources and Development of Mathematical Software*, edited by W. J. Cowell (Prentice-Hall, Englewood Cliffs, NJ, 1984), p. 88.

[43] W. H. Press, S. A. Teukolsky, W. T. Vetterling, and B. P. Flannery, *Numerical Recipes, The Art of Scientific Computing*, 3rd ed. (Cambridge University Press, Cambridge, 2007).

[44] J. D. Hunter, Matplotlib: A 2D graphics environment, Comput. Sci. Eng. **9**, 90 (2007).